



– *Technical Report* –

---

**Registration No.**

OPSEC#6711

**Date of Report**

06/09/2022

**Title: Understanding the Effects of Bolted-Joint Attachments and Their Use in Underbody Blast Applications.**

**Author(s):**

**Victor Burgess, Ground Vehicle Survivability and Protection (GVSP)**

DISTRIBUTION STATEMENT A. Approved for public release. Distribution is unlimited.

OPSEC#: 6711

U.S. Army Combat Capabilities Development Command  
Ground Vehicle Systems Center  
Detroit Arsenal  
Warren, Michigan 48397-5000

Approved for public release. Distribution is unlimited.

# REPORT DOCUMENTATION PAGE

Form Approved  
OMB No. 0704-0188

Public reporting burden for this collection of information is estimated to average 1 hour per response, including the time for reviewing instructions, searching existing data sources, gathering and maintaining the data needed, and completing and reviewing this collection of information. Send comments regarding this burden estimate or any other aspect of this collection of information, including suggestions for reducing this burden to Department of Defense, Washington Headquarters Services, Directorate for Information Operations and Reports (0704-0188), 1215 Jefferson Davis Highway, Suite 1204, Arlington, VA 22202-4302. Respondents should be aware that notwithstanding any other provision of law, no person shall be subject to any penalty for failing to comply with a collection of information if it does not display a currently valid OMB control number. **PLEASE DO NOT RETURN YOUR FORM TO THE ABOVE ADDRESS.**

<b>1. REPORT DATE (DD-MM-YYYY)</b>		<b>2. REPORT TYPE</b>	<b>3. DATES COVERED (From - To)</b>		
<b>4. TITLE AND SUBTITLE</b>			<b>5a. CONTRACT NUMBER</b>		
			<b>5b. GRANT NUMBER</b>		
			<b>5c. PROGRAM ELEMENT NUMBER</b>		
<b>6. AUTHOR(S)</b>			<b>5d. PROJECT NUMBER</b>		
			<b>5e. TASK NUMBER</b>		
			<b>5f. WORK UNIT NUMBER</b>		
<b>7. PERFORMING ORGANIZATION NAME(S) AND ADDRESS(ES)</b>			<b>8. PERFORMING ORGANIZATION REPORT NUMBER</b>		
<b>9. SPONSORING / MONITORING AGENCY NAME(S) AND ADDRESS(ES)</b>			<b>10. SPONSOR/MONITOR'S ACRONYM(S)</b>		
			<b>11. SPONSOR/MONITOR'S REPORT NUMBER(S)</b>		
<b>12. DISTRIBUTION / AVAILABILITY STATEMENT</b>					
<b>13. SUPPLEMENTARY NOTES</b>					
<b>14. ABSTRACT</b>					
<b>15. SUBJECT TERMS</b>					
<b>16. SECURITY CLASSIFICATION OF:</b>			<b>17. LIMITATION OF ABSTRACT</b>	<b>18. NUMBER OF PAGES</b>	<b>19a. NAME OF RESPONSIBLE PERSON</b>
<b>a. REPORT</b>	<b>b. ABSTRACT</b>	<b>c. THIS PAGE</b>			<b>19b. TELEPHONE NUMBER (include area code)</b>

# Understanding the Effects of Bolted-Joint Attachments and Their Use in Underbody Blast Applications

by

Victor Wilhelm Burgess

A thesis submitted in partial fulfillment of the requirements for the degree of Master of Science in The  
University of Michigan

Naval Architecture and Marine Engineering

2022

## Acknowledgements

This work was supported by the U.S. Army Ground Vehicle System Center (GVSC) Ground Vehicle Survivability and Protection (GVSP).

Thank you to my adviser, Nickolas Vlahopoulos, for your guidance and support throughout the master's degree program. From providing technical guidance to class selection, your support has greatly impacted my experience over the past three years.

Thank you to my Branch Chief, Rick Rickert, for your technical guidance and flexibility throughout this program. Your input has benefitted this project and has been greatly appreciated. Allowing me to appropriately balance work and school has enabled me to have adequate time to learn and complete my regular workload with minimal impact of my schooling while still working full-time.

Thank you to my fellow colleague Sanjay Kankanalapalli for your support learning all the simulation tools required to complete this project, as well as helping me setup and utilize the High-Performance Computing (HPC) systems through the Department of Defense networks.

Thank you to my wife Erin. Balancing the time obligations between work and school was only possible with your love and support. You and the rest of our family are the most important thing to me, and I am thankful for every day I spend in the life we built together.

## Table of Contents

Acknowledgements.....	2
Introduction .....	7
Approach.....	9
Test Apparatus and Environment .....	10
Threat and Threat Emplacement .....	12
Bolts and Bolted Joints.....	13
Measurements, Instrumentation, and Comparison Parameters.....	15
Measurement and Instrumentation .....	15
Parameters for Comparison.....	18
Modeling and Simulation.....	21
Simulation Environment .....	21
Material Selection and Fixture Meshing.....	22
Simulation Results and Analysis.....	26
Live Fire Testing .....	35
Test Setup .....	35
Testing.....	36
Results.....	37
Results Summary, Comparisons of Testing to Simulation, and Analysis .....	43
Conclusions .....	47
Future Work.....	49
Works Cited.....	50
Appendix A: Strainert Strain Gauge Calibration Example .....	51
Appendix B: Jump Height Curve Fit Analysis.....	53

**List of Figures**

Figure 1: GVSP blast coupon fixture showing a triangular structure to mitigate the loading and white covers to protect interior instrumentation. .... 10

Figure 2: Center cross section of fixture showing the target plate and attachment location, interior instrumentation mounting, and reference measurement location, and the test mast configurations..... 11

Figure 3: C4 explosive charge positioned in steel containment cylinder prior to a test event with top surface flush with top surface of steel containment cylinder. .... 12

Figure 4: (a) Full-Bridge strain gauge schematic showing the internal design of the instrumented bolt. (b) Strain gauge instrumented Grade 8 bolt with 23m cable used in testing with the connector coming out of the shank side of bolt..... 15

Figure 5: Instrumented bolt wiring diagram and test setup showing the connection points from the fixture through the precision filter and into the Dewetron DAS. .... 16

Figure 6: (a) ALE mesh configuration with the soil shown on the bottom in pink and the air on the top shown in blue. (b) Soil, Explosive, and Fixture in ALE environment during the detonation event and the explosive covering up the steel containment cylinder that is flush with the ground surface..... 21

Figure 7: (a) Node locations used for jump height calculations centered directly under each test mast mount location..... 25

Figure 8: Blast timeline description showing the peak of each perspective measurement and the time at which the peak occurred. The fixture displacement is tracked for initial movement not the peak in this case. .... 27

Figure 9: (a) Fringe plot of target plate at peak deformation showing the stress distribution. (b) Stress plot of Grade 8 bolts showing 4 failures in the center bolts and high tensile stresses on the 4 outer bolts. .... 28

Figure 10: (a) Fringe plot of the Grade 5 simulation target plate at peak deformation showing the stress distribution. (b) Stress plot of Grade 5 bolts showing 8 failures at the head of the bolt and 8 failures around nut threads. .... 28

Figure 11: (a) Fringe plot of the Grade 2 simulation at peak deformation showing the stress distribution. (b) Stress plot of Grade 2 bolts showing 8 failures at the head of the bolt and 8 failures around the nut threads. .... 29

Figure 12: Dynamic and permanent deformation comparison between bolt grades. The Grade 8 dynamic deformation shows to be less than the Grade 5 and Grade 2, but the permanent deformation appears similar between all three grades. .... 30

Figure 13: (a) Jump height curve fit data based on fixture displacement with the data points collected through  $t=0.050s$  for each and the curve fit tracking the full flight of  $t=0.5-0.6s$ . (b) Simulation peak jump height comparison. (c) Simulation peak velocity comparison. Both showing a reduction in jump height and velocity for the Grade 8 compared to the Grade 5 and 2..... 32

Figure 14: (a) Grade 8 bolt stresses showing loading just above UTS in some bolts with the loading occurring to  $0.002s$ . (b) Grade 5 bolt stresses exceeding UTS and the loading ending at  $0.001s$ . (c) Grade 2 bolt stresses showing loads well over UTS with the loading ending at  $0.001s$ ..... 34

Figure 15: (a) Grade 8 bolts showing some failure in the center bolts with remaining stress in some bolts shown in yellow and orange on the shank of the bolt. (b) Grade 2 bolts showing multiple failures at the head and in the shank of the bolts. .... 34

Figure 16: (a) Instrumented bolts, shown with brass connector at the tip of the shank, compared to dummy bolts with just the hole drilled and no strain gauge mounted. (b) Bolt loads observed during torquing process with proof loads indicated for each grade. The Grade 8 bolts showed the largest variation and the Grade 2 showing the least variation compared to the target proof load. .... 35

Figure 17: (a) Test 1 back face of deformed target with no failure observed. (b) Test 1 strike face of deformed target showing deformation and warping of the target plate. (c) Instrumented grade 8 bolts deformed after test showing yielding but no failures. (d) Bolt loads recorded during Test 1 showing an initial ramp up and then clipping due to the yielding of the bolts. .... 37

Figure 18: (a) Test 2 back face of deformed target showing permanent deformation but no failure. (b) Test 2 strike face of deformed target showing warping and some broken bolts. (c) Instrumented grade 5 bolts deformed after test showing failures in the center bolts and yielding on the remaining. (d) Bolt loads recorded during Test 2 showing yielding and the fracture of bolts 4 and 5 indicated by the flat line in the negative direction. .... 38

Figure 19: (a) Fixture after Test 3 showing target plate on ground after landing. The target centered under the fixture after the event indicates a strictly vertical flight of the fixture. (b) Deformed target plate after falling off fixture with no failures observed. (c) Failed instrumented grade 2 bolts after test with all bolts failing due to tensile failures. (d) Close in view of Grade 2 bolts showing ductile tensile failures indicated by necking and cup failure surfaces. .... 39

Figure 20: (a) Test 4 back face of deformed target showing no failures of the plate. (b) Test 4 strike face of deformed target showing warping and multiple bolt failures. (c) Instrumented Grade 8 bolts deformed after test. (d) Dummy bolts that fractured during the test showing failures at the center and outer edges. .... 40

Figure 21: Bolt loads recorded during Test 4 showing clipping at the yielding of the bolts event when the stresses were below the yield stresses of the bolts. .... 41

Figure 22: Comparison of permanent deformation recorded during test series indicating small differences between each test. .... 41

Figure 23: (a) Example of jump height curve fit analysis showing the data points collected throughout the event and the curve fit based on the test data. (b) Curve fit jump height comparisons from testing. (c) Peak velocity comparison of test series. Showing the highest jump height and largest velocity in Test 3 when the target plate fell off. (d) Impulse comparison from test series accounting for the target falling off during Test 3. .... 42

Figure 24: (a) Deformation comparison between test and simulations. (b) Velocity comparison between test and simulations. .... 44

Figure 25: Impulse comparison between test and simulations. .... 44

Figure 26: Combined test and simulation energy comparison. .... 45

Figure 27: Strainert strain gauge bolt calibration example. Calibration performed using SAE unit system and loads converted to SI during analysis stage. .... 52

Figure 28: (a-d) Jump height analysis for each test. Showing (a) the Grade 8, (b) the Grade 5, (c) the Grade 2, and (d) the Grade 8 High Torque. .... 54

**List of Tables**

Table 1: Bolt Parameters with Respect to Grade..... 13

Table 2: Bolt Torque Calculations Using Equation 2 ..... 14

Table 3: Strain Energy Material Properties ..... 20

Table 4: Material Properties for Fixture and Bolts used in Simulations ..... 22

Table 5: Bolt Load and Torque Adjustments for Testing ..... 36

Table 6: Standoff Measurements for each Test Number. .... 36

Table 7: Summary of Permanent Deformation Values from Testing..... 41

Table 8: Energy Breakdown for Test and Simulation..... 46

## Introduction

Military ground vehicles are required to function in many different environments and threat engagements around the globe. As such these vehicles need to protect its occupants against a multitude of threat engagements. One type of engagement is mine warfare. This consists of an opponent either burying an explosive device relative to the ground surface or surface laying an explosive device with the intent of detonating said device underneath the vehicle. This became extremely useful in World War 1 when the use of the first tanks were developed. Tanks changed the way wars were fought in a very large way by enabling a mobile gun protected by armor to traverse terrains traditionally handled by horse or on foot. This created the need for more powerful mines to counter the armor structure of a tank. During World War 2, anti-vehicle mine technology was enhanced further, and new tactics were developed to utilize them. As a result, military vehicles began including underbody armor into their designs to counter these attacks. As the years passed, military vehicles began getting lighter and more mobile. As a result, new armor materials were developed and integrated into the new combat vehicle designs. With an increase in vehicle capability also came an increase in mine technology, both in explosive size and function. In the 1960's there was a large push for the use of aluminum alloys in armor vehicles. The vehicles would be lighter, enhancing transportability and mobility. However, the aluminum was weaker than the armor steel used previously and thus required additional thickness to maintain equivalent performance. When the U.S. entered Vietnam, conventional mine warfare changed. There was a drastic need to protect these lightweight mobile vehicles against an unconventional enemy that was continuously changing their tactics and use of mines and explosives. From this emerged the use of vulnerability reduction kits for armored personnel vehicles. As vehicle designs matured through the 1980's and 1990's some mine enhancements were made. However, these were often traded for weight and mobility. As a result, most vehicles have base mine protection levels and the ability to add a mine protection kit or underbody kit to the vehicle for enhanced protection. In recent years during the Global War on Terror conducting operations in both Iraq and Afghanistan, U.S. troops were engaged in unconventional warfare which included the use very large Improvised Explosive Devices (IEDs) that were buried under and along transport roads. As a result, the mine protection of the vehicles had to be rapidly enhanced. This type of warfare tested most of the current underbody kit technologies and drove the need for a special class of vehicles known as Mine Resistant Ambush Protected (MRAP) vehicles. These vehicles were high off the ground with underbody kits that had aggressive "V" shapes to deflect the blast away from the occupants. While large efforts were made in the

development of underbody protection materials, mechanisms, and shapes, less work was focused on the integration or attachment of those kits on to the different military vehicles.<sup>[1]</sup>

The integration of an underbody kit can be approached in many ways. One method involves designing the protection into the hull structure. This makes the underbody protection a permanent part of the vehicle. This drives up the weight of the platform and in some cases reduces the mobility. A second method is to weld or fuse the underbody kit to the bottom of the vehicle. This semi-permanent method requires the underbody kit to be made of a similar material as the vehicle hull structure with the ability to add the kit later when it is needed. The final and most common method is the use of non-permanent attachments such as screws and bolts. This enables a wide array of materials and mechanisms to defeat all different types of mines. This also enables theater-specific kits to be developed based on the type of mine warfare being used. Finally, the use of non-permanent attachments enables future upgrades to the system as new materials and mechanisms get developed.

The use of screws and bolts enable a large amount of flexibility. However, it also identifies a large amount of design related unknowns: How strong does the attachment point need to be? How much load do the bolts take during the blast event? Do they just need to hold the kit in the correct position for the mine engagement or do these bolts need to stay on for the entire engagement? Can the bolted joint alter the boundary conditions of the underbody kit and the hull structure such that it reduces the intrusion into the vehicle occupant area or reduces the global vehicle response of the mine onto the vehicle structure? The focus of this effort is to determine the effect of bolt strength on the underbody kit interface to the hull structure with respect to the intrusion caused by deformation into the occupant area and the global response on the vehicle structure to enable more efficient underbody kit designs for increased occupant protection in ground vehicles.

## Approach

For this study, a combination of simulations and live fire testing will be conducted. The simulations will be used to understand the changes in performance at a theoretical level and the live fire testing will realize these results and verify the simulation assumptions with practical application.

The first part of the effort is to understand the different types of common bolts that are used and how they attach an underbody kit to the hull structure. The second part of the analysis requires the use of a controlled and repeatable test apparatus that can also be modeled in the simulation environment. Then, a set of common measurements or parameters can be applied to both the simulations and testing needs to be determined. Finally, a comparison of the simulation results and test data will be made to understand and quantify the differences observed.

All calculations and data are presented using the International System of Units (SI) or the metric measurement system. Depending on the unit system used for each equation or instrumentation system, some calculations are performed using English units and are converted to SI during the analysis stage. The specification used for the bolts selected follow the Society of Automotive Engineers (SAE) J429 Grading system for cap screws, as this is one of the more commonly used standards of bolts and the units were converted for consistency.

## Test Apparatus and Environment

This study required the use of a consistent fixture or structure that would provide repeatable results during testing and was able to be accurately modeled in the simulation environment. Ground Vehicle Survivability and Protection (GVSP) already has a blast coupon test fixture that has been used previously in other research efforts<sup>[2]</sup> that have included both simulation and testing. Figure 1 shows a CAD image of the GVSP blast coupon fixture that will be used for this effort.

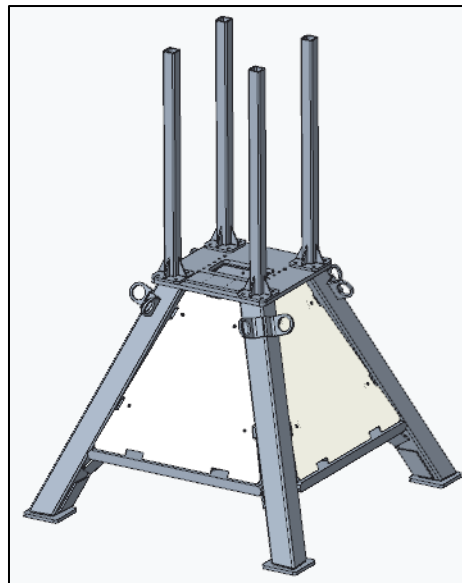
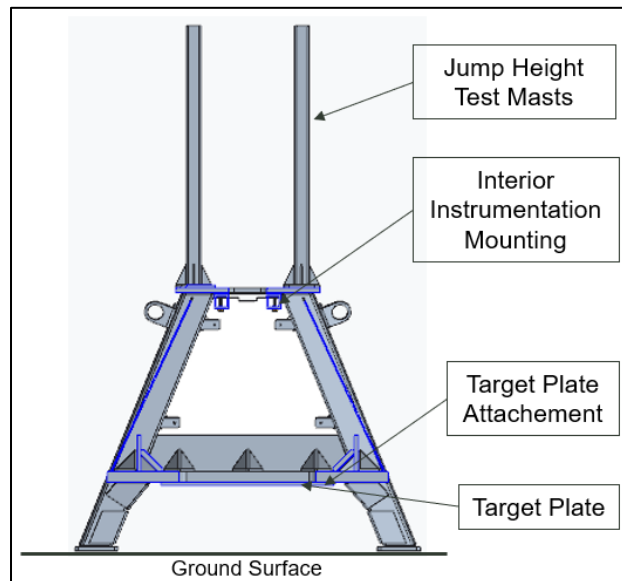


Figure 1: GVSP blast coupon fixture showing a triangular structure to mitigate the loading and white covers to protect interior instrumentation.

OPSEC# 6711

The fixture is designed to use a 1.219m by 1.219m target that is attached to the fixture using 16, 25mm diameter through bolts with nuts attached to the opposite side. The target mounts to the bottom side of the fixture which is suspended above an explosive emplacement to provide an upward load indicative of an underbody blast event. The target thickness, material type, distance from the explosive threat, and explosive threat emplacement are all variable and can be modified specifically for each experiment. Figure 2 shows a cross section view of the fixture indicating the ground surface, target plate, target plate attachments, interior instrumentation mounting, and jump height masts.



**Figure 2: Center cross section of fixture showing the target plate and attachment location, interior instrumentation mounting, and reference measurement location, and the test mast configurations.**

The target material selected is Rolled Homogenous Armor (RHA) steel with a specified thickness of 25.4mm. This is held constant through both the simulations and testing. During the testing, a new target is replaced for each test. They are all fabricated at the same time using the same manufacturing lot of material.

## Threat and Threat Emplacement

Conventional landmines are traditionally buried in soil as to conceal their presence. Therefore, testing usually involves the preparation of a soil test bed to specific Army standards for consistency. Due to the nature of the soil interaction, even when the standards are followed, there is a 15-25% test-to-test variation observed during testing. For this study the focus is on a consistent response of the explosive on the target and fixture. As such an alternative method for threat emplacement is used. A steel containment cylinder is fabricated such that a large pocket is machined in the top of the cylinder to hold the explosive charge. This directs the blast load upward but isolates the explosive from the soil. The steel containment cylinder is then buried in the ground such that the top surface is flush with the ground surface. This provides a consistent emplacement that can be repeated for each test. The steel containment cylinder is inspected between each test, and it is replaced if cracking is observed. The explosive used for this study is Composition C4 as it is readily available and very stable. The C4 is packed into a plastic mold to control the shape of the threat. Figure 3 shows the C4 threat (shown in a white plastic mold) placed in the steel containment cylinder and denotated using an electronic blasting cap on the lower 1/3 section of the C4 along the axis of the cylindrical shape.



Figure 3: C4 explosive charge positioned in steel containment cylinder prior to a test event with top surface flush with top surface of steel containment cylinder.

## Bolts and Bolted Joints

Bolted joints are used in many structural applications for static and dynamic load conditions. An underbody kit has two major load profiles: low amplitude-high cycle, and dynamic single impulse events. The low amplitude-high cycle loading is observed in regular vehicle operations where the vehicle is driving around, and the underbody kit sees vibrations from road loads. The dynamic single impulse event is a result of an explosive load imparted on the bottom of the vehicle during a mine engagement event. The low amplitude, high cycle loading is very well understood. However, there is less information on the explosive loading of bolts in vehicle applications.

Bolt sizes and grades determine the specified strength and load capability. Leveraging the data collected from the specifications, three bolt grades are evaluated: Grade 8, Grade 5, and Grade 2. Bolt engineering specifies four major parameters for each bolt: minor diameter, minimum proof strength, minimum tensile strength, and minimum yield strength. These parameters are used to determine the design loads and bolt size for each application. 25.4mm nominal diameter bolts are used for this study. All three grades of bolts selected are medium grade carbon steel. For the purposes of this study, the Elastic Modulus is assumed to be constant for the calculations and simulations. Table 1 shows a summary of the bolt parameters used for the calculations. This data is duplicated from a mechanical engineering design handbook<sup>[3]</sup>.

**Table 1: Bolt Parameters with Respect to Grade**

<b>Bolt Grade Specification Parameters</b>			
<b>Bolt Grade</b>	<b>8</b>	<b>5</b>	<b>2</b>
<b>Minor Diameter (mm)</b>	21.50		
<b>Minimum Proof Strength (MPa)</b>	827.37	586.05	227.53
<b>Minimum Tensile Strength (MPa)</b>	1034.21	827.37	413.69
<b>Minimum Yield Strength (MPa)</b>	896.32	634.32	248.21
<b>Elastic Modulus (MPa)</b>	210000.00		

To determine the specified bolt torque value for each grade of bolt, the axial load is required. For each of the bolts selected the axial load was 70% of the proof load determined from the minimum proof strength of each bolt. The minimum proof load is determined using equation 1 below. Once the proof load was determined for each bolt grade, the required torque was determined using equation 2. It has been stated that for torque values, there is a  $\pm 30\%$  error in application<sup>[4]</sup>. Table 2 shows the values used for each calculation. This data will be used as the baseline for both the simulations and testing for this effort.

$$W_{proof} = \sigma_{proof} * A_{bolt\ minor} \quad (1)$$

$$\frac{PL}{W} = \mu_b R_b + R_t \left( \mu_t \sec(\alpha) + \frac{1}{2\pi N R_p} \right) \quad (2)$$

Where:  $P$ =force applied to the wrench (N)

$L$ =length of the wrench (m)

$W$ =total tensile force in the bolt (N)

$\mu_b$ =effective coefficient of friction on bearing face (0.15 used)

$R_b$ =effective radius of action of friction forces  $\left( \frac{2}{3} \frac{(R_o^3 - R_i^3)}{(R_o^2 - R_i^2)} \right)$  where  $R_o$  and  $R_i$  are outer and inner radius

$R_t$ =effective radius of action of frictional forces (=pitch radius)

$\mu_t$ =effective coefficient of friction between thread flanks (assumed to be equal to  $\mu_b$ )

$\alpha$ =angle between mating faces (30 degrees)

$N$ =thread pitch,  $R_p$ =pitch radius<sup>[5]</sup>

Note: Certain digits carried through unit conversions of English to Metric.

**Table 2: Bolt Torque Calculations Using Equation 2**

<b>Bolt Torque Calculations</b>			
<b>Grade</b>	<b>8</b>	<b>5</b>	<b>2</b>
$W$ (N)	210335.2	148987.4	57842.2
$\mu_b$	0.1500000	0.1500000	0.1500000
$R_b$ (m)	0.0116515	0.0116515	0.0116515
$R_t$ (m)	0.0115722	0.0115722	0.0115722
$\mu_t$	0.1500000	0.1500000	0.1500000
$\alpha$ (rad)	0.5235990	0.5235990	0.5235990
$N$	314.9606	314.9606	314.9606
$R_p$ (m)	0.0115722	0.0115722	0.0115722
<b><math>PL</math> (N*m)</b>	<b>895.4827</b>	<b>634.3002</b>	<b>246.2577</b>

## Measurements, Instrumentation, and Comparison Parameters

### Measurement and Instrumentation

A common set of measurements, key parameters, and instrumentation are established to ensure comparable data is collected from both physical testing and simulations. The measurements are the initial target plate standoff from the threat, deformation of the target plate, and fixture jump height. For this study, deformation is defined as the maximum difference in displacement of the back side of the target plate before and after the explosive event. The initial standoff of the target plate is measured from the top surface of the steel containment cylinder to the impact surface of the target.

The initial torque value of the bolts is measured only during testing. Bolt torque is not measured in the simulations. Instead, an element along the center axis of the bolt is used to measure the stress. Special bolts with strain gauges mounted along the axis of the bolt shaft are utilized. They are used to measure the axial load of each bolt during the torquing process as well as during the tests. There are a total of 16 bolts used to hold the target plate to the fixture, eight bolts on each side. All the testing is symmetric down the centerline of the fixture with the threat placed directly in the center of the target plate. Therefore, only eight bolts are instrumented with the strain gauges. The instrumented bolts have a full-bridge strain gauge setup with 350-ohm resistors. Figure 4a shows the schematic of the strain gauge from the manufacturer's website<sup>[6]</sup>. Figure 4b shows the strain gauge instrumented bolt with cable.

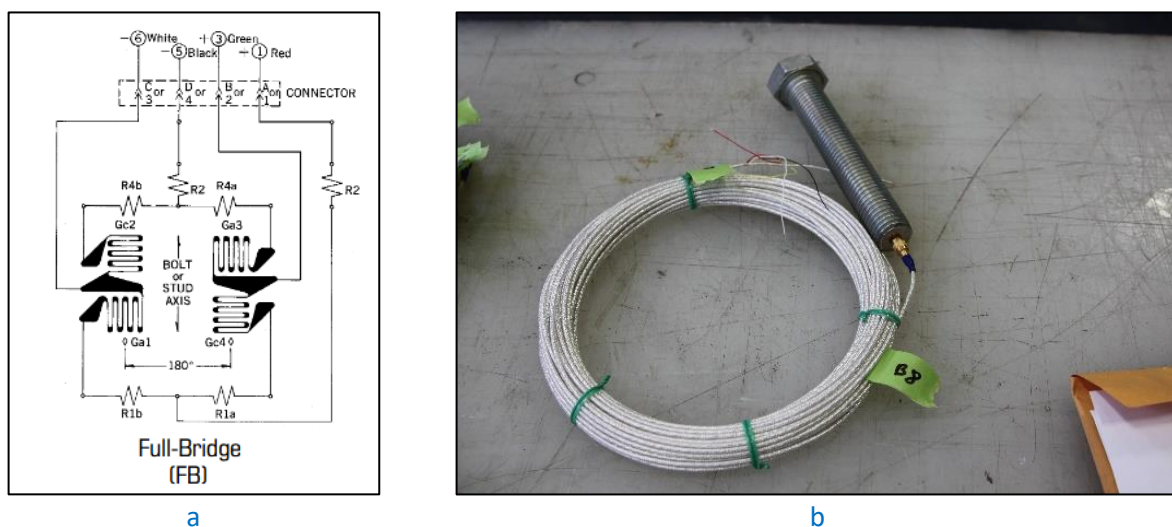


Figure 4: (a) Full-Bridge strain gauge schematic showing the internal design of the instrumented bolt. (b) Strain gauge instrumented Grade 8 bolt with 23m cable used in testing with the connector coming out of the shank side of bolt.

OPSEC# 6711

This bolt instrumentation system has been used for armor development testing<sup>[7]</sup> in the past. However, it has not been used for a blast test series prior to this test series. Due to the large debris field surrounding the event, some modifications to the current setup are required. The first is the length of the cabling from the instrumented bolts to the green junction box which converts the strain gauge cable to a DB9 serial cable. Conventionally, a 4.5m cable is used. This must be extended to 23m to get the instrumentation system out of the blast radius. For high-speed data collection applications, it is not recommended to use an extended cable length. The manufacturer of the strain-gauge bolts was consulted. The solution is to perform the calibration of the strain gauge instrumented bolt with the extended cable attached to ensure accuracy. Appendix A shows an example of the strain gauge bolt calibration sheet. Figure 5 shows the instrumentation setup for the test series. The major components of the system are the bolts attached to the fixture, which are ran with the 23m cables to the green junction box where they are converted to serial DB9 cables and attached to a Precision Filter signal conditioner, and then connected to the Dewetron 3210 Digitizer and Reorder Data Acquisition System (DAS). The Precision Filter signal conditioner is used to apply the excitation voltage and balance the bridged system prior to logging the data using the Dewetron system. For this test series the maximum sample rate of the system, 10 MHz, is utilized to ensure as much data as possible is collected. Prior to the test series, it is unknown what sample rate is required to capture the load data because bolt load data has not been monitored during a blast test event used for vehicle structure applications. The Dewetron system triggers off a minimum load specified from any one of the bolts. Therefore, the timeline from blast detonation cannot be established during the testing as was performed with the simulations.

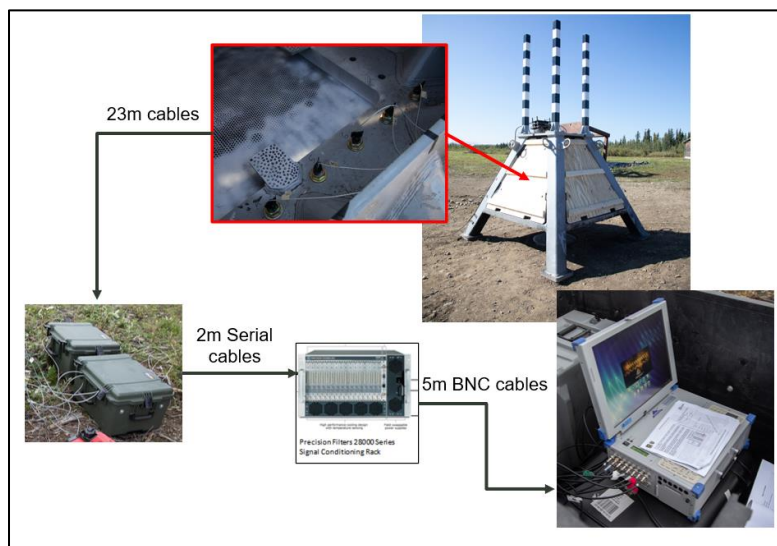


Figure 5: Instrumented bolt wiring diagram and test setup showing the connection points from the fixture through the precision filter and into the Dewetron DAS.

The deformation of the target plate is measured from the back surface for both the simulation and testing. During the blast event there are two different stages of deformation of the target plate, the first is the peak dynamic deformation which is the initial elastic-plastic response of the target. This usually occurs in the first 3-6ms of the event. Then the target plate rebounds into a purely plastic state which is referred to here as permanent deformation. Only the permanent deformation was measured after each test. The data was collected by measuring a point of reference on the fixture to the back side of the target plate before and after the test. If a target plate falls off the fixture during a test, reference locations around the perimeter of the plate where it attaches to the fixture are used. For the simulations, both the dynamic and permanent deformation can be measured. This is performed by monitoring the nodal displacement of a node located on the back surface of the target plate directly above the threat location.

The fixture jump height measures the vertical displacement of the fixture during the test event. During the live fire testing, two Photron FastCam SA2 high speed video cameras with a frame rate of 5000 frames per second (fps) are placed orthogonally to each other with one camera facing the south side of the fixture and one facing the west side of the fixture. On the top of the fixture there are 4 test masts that are mounted with 152.4mm tall alternating black and white stripes. This known measurement value is used to determine a distance per pixel value for each test mast location. During the event points of the test masts are tracked. Next, a displacement in pixels is measured and then converted into a distance. This establishes a time-based trajectory of the fixture for each event. On the simulations, the jump height is measured using four reference nodes at the base of the fixture mast mounts. These are plotted as nodal displacements.

## Parameters for Comparison

Using the measurements from above, a series of parameters are established to compare all the tests to each other, all the simulations to each other, and then compare the tests to the simulations. The first parameter is deformation. The permanent deformation is compared and is a direct measurement of the target plate. Next, the global motion of the fixture needs to be determined. Using the jump height trajectory,  $d_{fixture}$ , the vertical displacement of the fixture. A second order, parabolic curve fit of the data points is performed using MATLAB<sup>[8]</sup>. Using equation 3, a velocity curve is established.

$$v = \frac{d}{dt}(d_{fixture}) \quad (3)$$

The next parameter for comparison is the peak velocity observed based on this velocity curve, and is referred to as the global velocity,  $v_{global}$  of the fixture. The next parameter used for comparison is the impulse. The impulse is determined using equation 4 below. However, the mass used in the equation needs to be broken up into two components: the mass of the target plate,  $m_{target}$  and the mass of the fixture,  $m_{fixture}$ .

$$I = (m_{target} + m_{fixture}) \times v_{global} \quad (4)$$

If the target plate falls off during the event, only the mass of the fixture is used. The mass of the fixture without the target plate is 3779.55kg and the mass of the target plate is 293.18kg. Therefore, the mass of the target plate compared to the total combined mass is 7.20%. Conventional military vehicles underbody kits contribute 3-11% of the overall Gross Vehicle Weight (GVW), showing relevance of the target plate and fixture mass separation compared to the underbody kit staying on or falling off during the event. If other items such as bolts or other small components separate from the fixture during an event, these are considered negligible. For this study the threat and the standoff to the threat are held constant. Therefore, the impulse imparted on the target plate is expected to be the same from test to test.

The final parameter used for comparison is total energy. The total energy calculations account for the energy absorbed by the target plate itself during the deformation process, the energy absorbed by the bolts during the initial loading, and the kinetic energy of the fixture during its displacement. Determining the energy absorbed in the target plate during the deformation process is non-trivial. For this study, it is assumed that the energy absorbed is strictly from the elastic response of the material, where strain energy ( $U_t$ ) equations can be used. Leveraging previous work performed by P.S. Westine, and others at the Southwest Research Institute<sup>[9]</sup>, an equation for strain energy of a beam that is clamped on each end with no rotation but can move inwards was determined to be the most relevant for this application. Using this equation and the mechanical material properties of the target plate shown in Table 3 an equation for energy absorbed is derived as a function of deformation of the target plate, which is shown in equation 5. The energy equation for the bolts is also assumed to be the elastic strain energy ( $U_b$ ) capable based on the material properties. A conventional strain energy equation is used<sup>[3]</sup> for equation 6. The kinetic energy of the fixture is determined using equation 7 below. Like the impulse equation, the mass of the target plate is omitted if the target plate falls off during the event. Equation 8 shows the total energy equation as the summation of the three energy components.

$$U_t = \frac{16M_y w_o}{L} \quad (5)$$

Where  $M_y = \frac{\sigma_y b h^2}{4}$  and  $\sigma_y$  is the yield stress of the target plate material

$b$  = the width of the target plate

$h$  = the height of the target plate

$L$  = the length of the target plate

$w_o$  = the deformation of the target plate

$$U_b = \frac{S_y^2}{2E} \forall \quad (6)$$

Where  $S_y$  = the yield stress of the bolt

$E$  = the elastic modulus of the bolt

$\forall$  = the volume of bolts

$U_b$  is the summation of the 16 total bolts adhering the target plate

$$E_f = \frac{1}{2} (m_{target} + m_{fixture}) \times v_{global}^2 \quad (7)$$

$$E_{tot} = U_t + U_b + E_f \quad (8)$$

Table 3: Strain Energy Material Properties

Strain Energy Material Properties	
Target Plate	
$\sigma_y$ (MPa)	855.00
$b$ (m)	1.219
$h$ (m)	0.0254
$L$ (m)	1.219
Bolts	
$S_y$ (MPa) Grade 8	824.00
$S_y$ (MPa) Grade 5	586.00
$S_y$ (MPa) Grade 2	228.00
$E$ (Pa)	210000.00
$\forall$ (Volume of 16 bolts) (m <sup>2</sup> )	2.62E-04

## Modeling and Simulation

### Simulation Environment

The simulations for the project are ran using Livermore Software Technology Corporation (LSTC) LS-DYNA<sup>[10]</sup> simulation software leveraging their Arbitrary Lagrangian Eulerian (ALE) method. All the meshing work was performed using Altair's Hyperworks Hypermesh software<sup>[11]</sup>. The ALE method is used to allow the explosive interaction to behave as a fluid through the different mediums. This fluid interaction is then applied to the target plate and blast fixture resulting in a Lagrangian response of the structure. The ALE setup was leveraged from previous projects<sup>[2]</sup> and modified to fit this experiment. The ALE environment includes the steel containment cylinder, the soil surrounding the cylinder, the air around the fixture, and the explosive. These were all meshed and divided using the volume fraction method. The Eulerian mesh is a cylindrical shape comprised of 4,094,781 nodes and 4,032,000 elements with a size of 10m in diameter and 6 m tall overall. The volume contains a 1m tall soil layer and a 5m tall air mesh above the ground surface. This is approximately 2.5 times with width of the fixture and accounts for 1m of jump height in the vertical direction to contain the fixture in the Eulerian mesh throughout the duration of the simulation. This was based on previous test series with this threat and fixture configuration. Figure 6a shows the air in blue and the soil in pink. With the air turned off in the model, the soil, fixture, and explosive products can be identified in Figure 6b. The steel containment cylinder is obscured by the explosive.

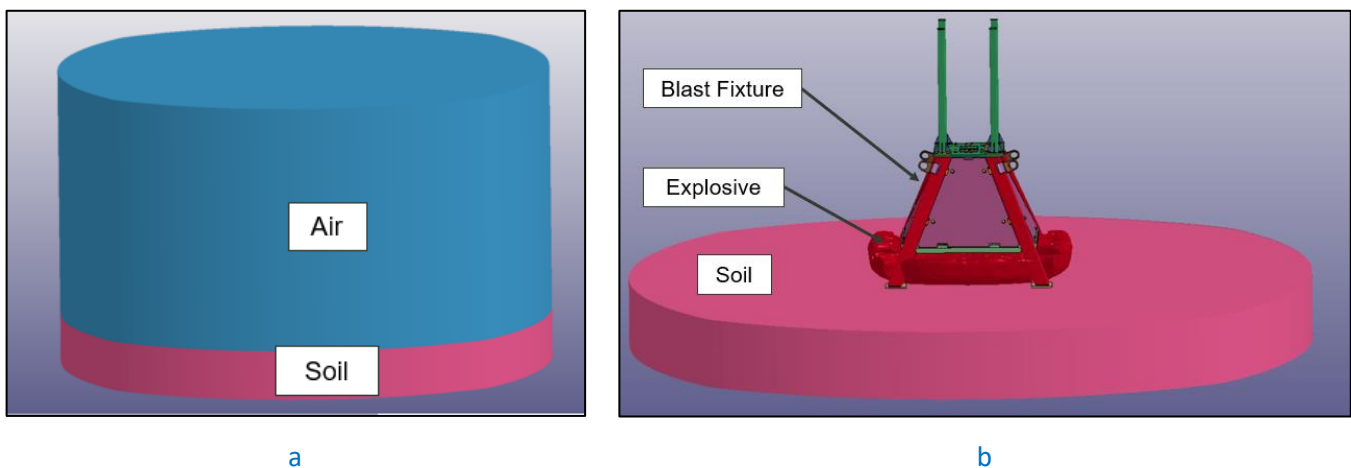


Figure 6: (a) ALE mesh configuration with the soil shown on the bottom in pink and the air on the top shown in blue. (b) Soil, Explosive, and Fixture in ALE environment during the detonation event and the explosive covering up the steel containment cylinder that is flush with the ground surface.

## Material Selection and Fixture Meshing

The soil used for the simulation leveraged a previous Silty Sand type soil. Since the explosive was contained in the steel cylinder, the soil did not impact the explosive loading on the target and fixture. For the explosive, a Jones-Wilkins-Lee (JWL)<sup>[12]</sup> equation of state (EOS) is used to describe the detonation products. Equation 9 shows the formula used to determine the resultant pressure throughout the detonation process. The specific values of this material model are excluded from this report. The air is modeled using a conventional linear polynomial EOS.

$$p = A \left(1 - \frac{\omega}{R_1 V}\right) \exp(-R_1 V) + B \left(1 - \frac{\omega}{R_2 V}\right) \exp(-R_2 V) + \frac{\omega e_0}{V} \quad (9)$$

Where  $A$ ,  $B$ ,  $R_1$ ,  $R_2$ ,  $\omega$ , and  $e_0$  are specific constants of the explosive.

$V = \frac{\rho_e}{\rho}$  where  $\rho_e$  is the density of the explosive and  $\rho$  is the density of the detonation products.

The fixture is comprised of mostly structural steel. It is modeled using a piecewise linear plasticity model, or MAT24<sup>[13]</sup> material card in LS-DYNA, which uses quasi-static material properties developed from experimental data. The MAT24 card is also used for the bolts with adjustments based on each bolt grade. Table 4 shows the material properties used for the fixture and each grade of bolt.

**Table 4: Material Properties for Fixture and Bolts used in Simulations**

Material	Density (kg/m <sup>3</sup> )	Elastic Modulus (MPa)	Poisson Ratio	Yield Stress (MPa)
Fixture (A514 Steel)	7850.00	210000.00	0.30	690.00
Grade 8 Bolt	7850.00	210000.00	0.30	896.00
Grade 5 Bolt	7850.00	210000.00	0.30	634.00
Grade 2 Bolt	7850.00	210000.00	0.30	248.00

The final material used is for the target plate. The material selected for the target plate is RHA. The target plate experiences a high strain rate elastic-plastic response due to the explosive loading. It is important to capture the material response in the simulation. A Johnson-Cook<sup>[14]</sup> constitutive material model is utilized so that the strain-rate, temperature, and failure of the specific material are all represented in the material model. Equation 10 shows the Johnson-Cook material model. Equation 11 shows the Johnson-Holmquist Damage Evolution Rule<sup>[15]</sup>. LS-DYNA uses both to represent that material properties through the high strain rate response and failure. The specific material constants are not included in this report.

$$\sigma_y = [A + B(\epsilon_{eff}^p)^N](1 + C \ln \dot{\epsilon})[1 - (T_H)^M] \quad (10)$$

Where  $\epsilon_{eff}^p$  is the effective plastic strain.

$$\dot{\epsilon} = \frac{\dot{\epsilon}_{eff}^p}{\dot{\epsilon}_0} \text{ where } \dot{\epsilon}_0 \text{ is the strain rate used to determine } A, B, \text{ and } N.$$

$$T_H = \frac{T - T_R}{T_M - T_R} \text{ is the Homologous Temperature, } T_M \text{ and } T_R \text{ are the Melt Temperature and Reference$$

Temperature when determining  $A, B, \text{ and } N.$

The model has five parameters:  $A, B, C, \text{ and } M$ , and three material characteristics  $\rho, C_p, \text{ and } T_M.$

$$\epsilon_f = D_1(p^* + T^*)^{D_2} \quad (11)$$

Where  $\epsilon_f$  is the strain to failure.

$p^*$  is the normalized stress.

$T^*$  is the normalized tensile hydrostatic pressure.

$D_1$  and  $D_2$  are material constants.

The actual fixture is comprised of a series of parts that are welded together. For the simulations, each part was meshed, and the welds were simplified to use *nodal ties* which rigidly link the nodes from two parts together. The nodes selected were along the weld path of each joint. The final fixture meshed model is comprised of 1,591,787 nodes and 1,290,590 elements. 2D Shell mesh elements were used for the angled square tubing and 3D solid elements were used for all the plate components. A minimum of 5 elements per thickness were used on the target plate, the bolts, and the frame that the target plate attaches to. Previous work shows that 3-5 elements per thickness is the recommended minimum mesh density for blast loading problems<sup>[16]</sup>. For computation efficiency, each simulation was run for 50ms. This allows for

enough time for the blast loading process on the target plate and lift off the fixture. However, it does not capture the entire flight. Instead, only the initial liftoff is captured.

Multiple debug simulations were performed to understand to functionality of the system. During which the default data collection frequency of 1200Hz was used. Using a Department of Defense (DoD) High Performance Computing (HPC) cluster, each simulation took approximately 27 hours to complete utilizing 32 cores. The number of cores used is dictated by the number of LS-DYNA licenses available. For this effort 32 licenses were allocated. This output frequency was able to capture the fixture displacement but was missing some of the deformation points. Target plate deformation during a blast event is approximately 150 to 200m/s. Knowing that the deformation occurs in the first 6ms of the event, a minimum sampling rate of 33 kHz is required. This was rounded up to 40kHz for the simulations. However, not all the data points required this sample rate frequency. Using the debug simulations, specific nodes and elements were identified in the model and since the fixture mesh and target plate is consistent for each simulation run, any nodes or elements identified from the fixture mesh and target plate would be that same for each subsequent simulation. Using the *BINOUT* keyword in LS-DYNA, multiple nodes and elements were selected to directly output values such as displacement and stress. This increases the sampling rate for each of these nodes without requiring a complete simulation step at the increased interval which is computationally expensive. For these simulations the *BINOUT* data was collected at 40kHz instead of the 1200Hz used in the rest of the model. This increased the run time from 27 hours to 38 hours per simulation at the 32 cores. Figure 7a shows the node locations on the top of the fixture used to record fixture vertical displacement or jump height. These nodes are located directly under the test mast mount plates. Figure 7b shows the node locations measuring the peak deformation of the target plate. Figure 7c shows a cross section of the blast fixture indicating the locations of the target plate elements used to measure the blast pressure imparted on the target plate. Figure 7d shows a cross section of the fixture showing the element in each bolt selected to measure the axial stress in the bolts.

OPSEC# 6711

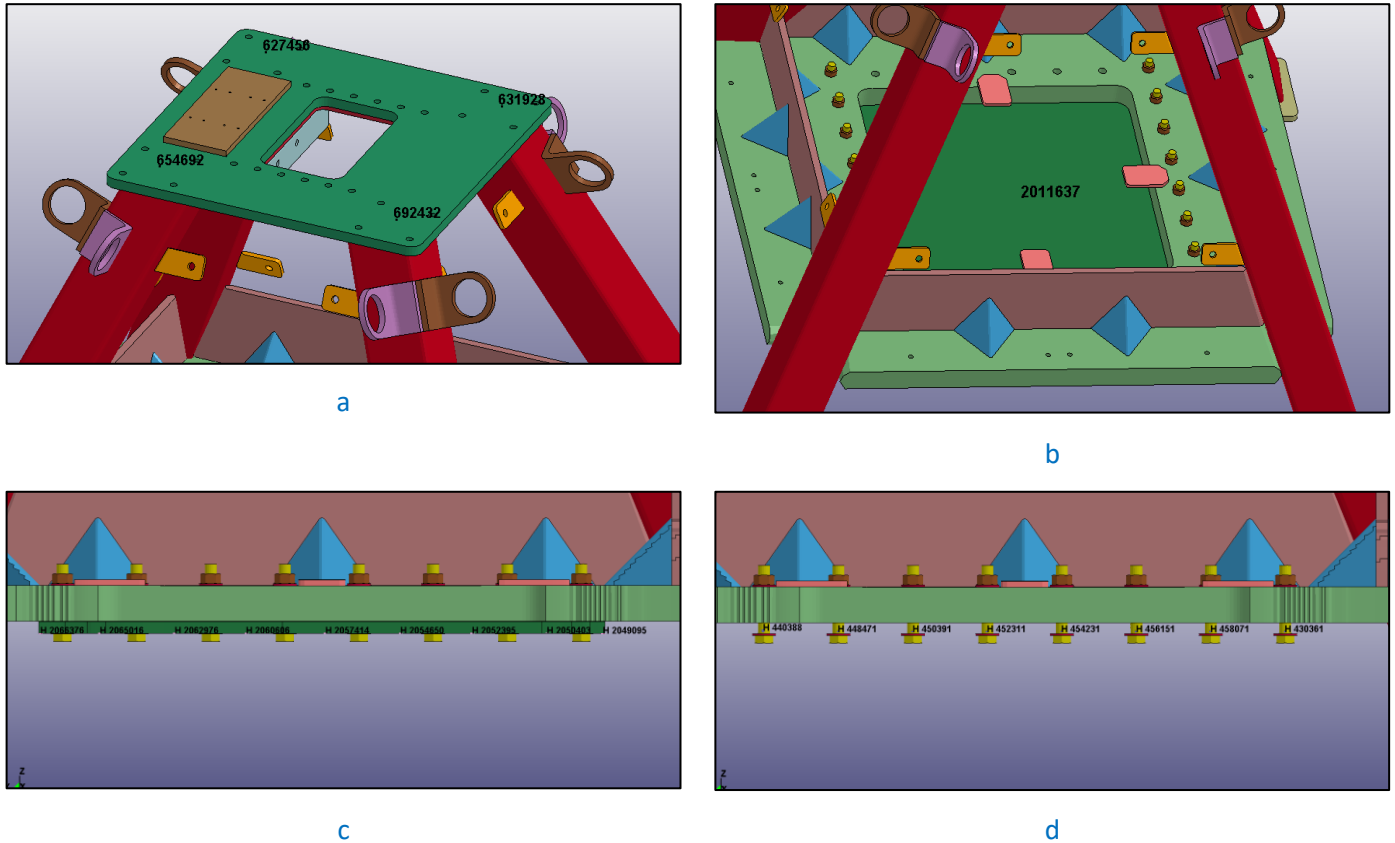


Figure 7: (a) Node locations used for jump height calculations centered directly under each test mast mount location. (b) Node location used for deformation measurements selected to be directly above the axis of the threat. (c) Target plate element locations for tracking blast pressures used to track the blast pressure distribution during the event. (d) Element locations used to measure bolt stresses at each bolt location corresponding to the instrumented bolt locations.

After the debugging process three simulations were performed with the only variable between each simulation being the bolt strength, adjusted from Table 4 above. Once the simulations were completed the data was collected using LS PrePost<sup>[17]</sup> and then processed through MATLAB.

## Simulation Results and Analysis

To provide a better understanding of the blast loading event, a timeline of the first 0.01 seconds is determined using the simulation data. The blast starts with detonation, the initial loading of the target plate, the bolt loading, the target plate deformation, and finally the fixture vertical displacement. Figure 8 shows these key areas on a common plot with time on the x-axis and each trace normalized to a unit factor for easy identification. The timeline shows the peak pressure directly above the charge loading the target plate at 0.33ms. This is immediately followed by the Grade 2 and Grade 5 bolt load peak stress at 0.57ms, and then the Grade 8 bolt load peak stress at 0.77ms. Here, it is observed the bolt stress peaks at approximately the same time the target plate deformation begins to occur. The peak deformation occurs at 1.90ms, almost 1.5ms after the initial blast loading, and then the fixture displacement begins as the target plate deformation has rebounded from the initial dynamic elastic-plastic response. From this timeline, the bolts are loaded well before the peak deformation, so if the bolts were to break from the initial stress load it would have minimal effect on the deformation. However, the Grade 8 bolt loading lasts significantly longer than the Grade 5 or Grade 2 bolts. Based on this data, it appears the Grade 5 and Grade 2 bolt failures happen when the peak load is observed at 0.57ms. Conversely, the Grade 8 bolts do not fracture until approximately 1.1ms. It is also clear then that the entire deformation event occurs before any significant global motion of the fixture and therefore the deformation and the global motion appear to be decoupled from each other.

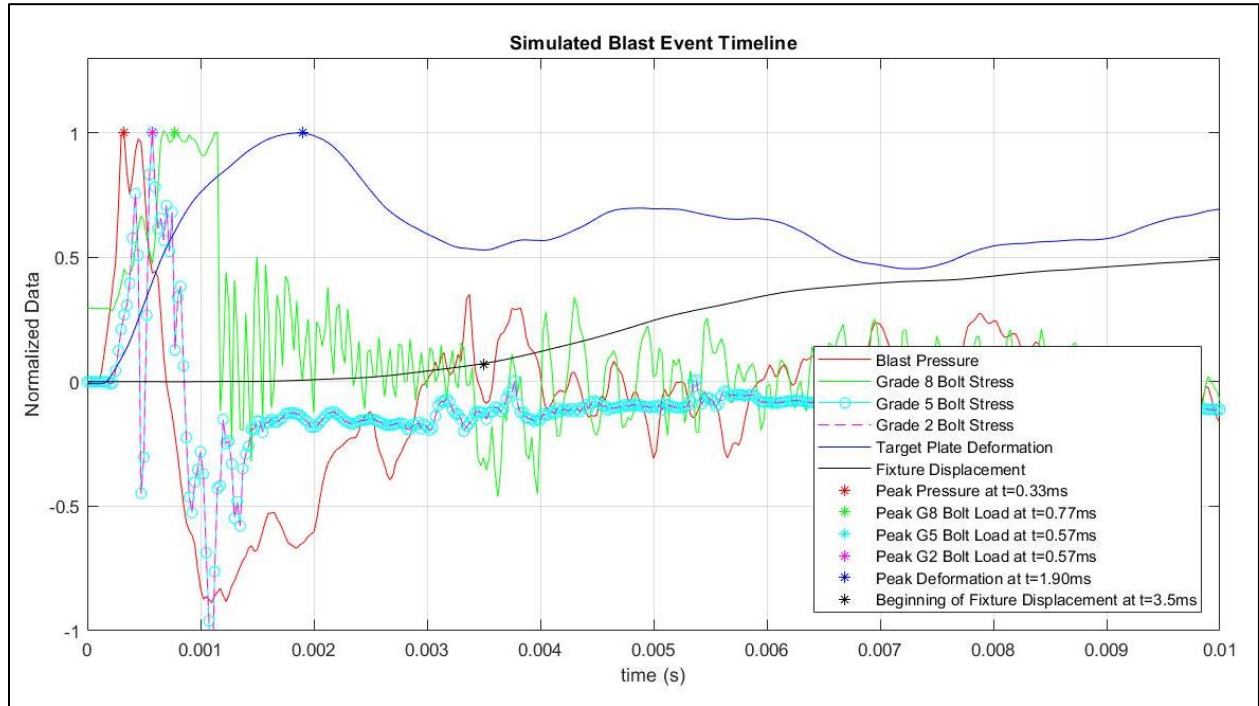


Figure 8: Blast timeline description showing the peak of each perspective measurement and the time at which the peak occurred. The fixture displacement is tracked for initial movement not the peak in this case.

The Grade 8 simulation did not show any target plate failure. Figure 9a shows a fringe plot of the Grade 8 simulation with the maximum acceptable failure strain of 13%. This is the maximum failure strain for the RHA material. 4 of the 16 bolts failed during the simulation. Figure 9b shows the stress plot of the bolts with the center two bolts on each side showing failure.

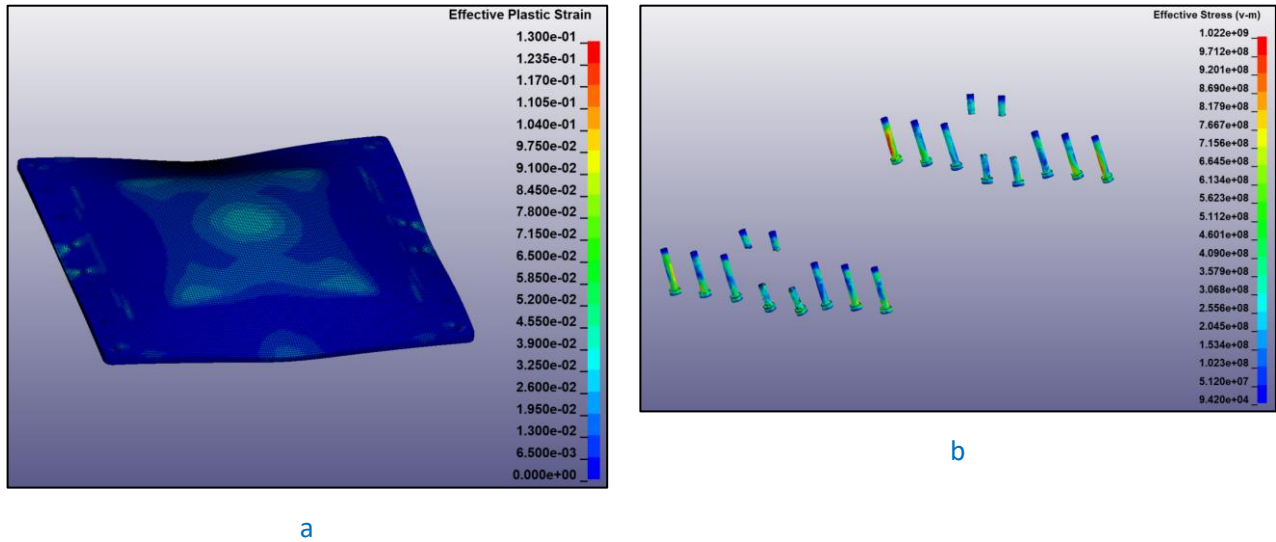


Figure 9: (a) Fringe plot of target plate at peak deformation showing the stress distribution. (b) Stress plot of Grade 8 bolts showing 4 failures in the center bolts and high tensile stresses on the 4 outer bolts.

The Grade 5 simulation did not show any target plate failure, but the target plate fell off during the simulation. Figure 10a shows a fringe plot of the Grade 8 simulation with the maximum acceptable failure strain of 13%. 16 of the 16 bolts failed during the simulation. Figure 10b shows the stress plot of the bolts with the center two bolts on each side showing failure.

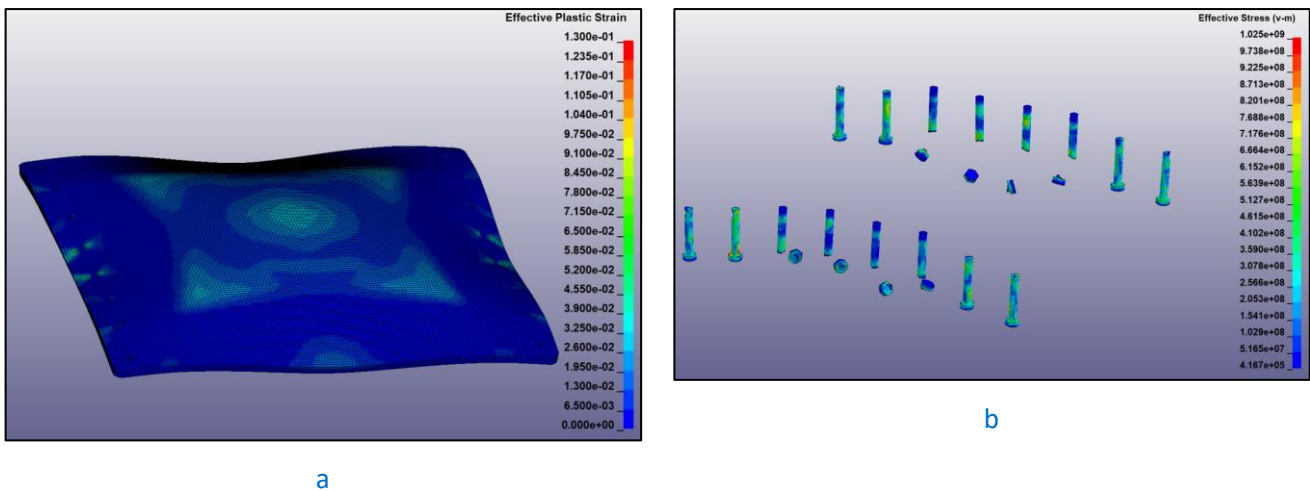


Figure 10: (a) Fringe plot of the Grade 5 simulation target plate at peak deformation showing the stress distribution. (b) Stress plot of Grade 5 bolts showing 8 failures at the head of the bolt and 8 failures around nut threads.

The Grade 2 simulation did not show any target plate failure, but the target plate fell off during the simulation. Figure 11a shows a fringe plot of the Grade 8 simulation with the maximum acceptable failure strain of 13%. 16 of the 16 bolts failed during the simulation. Figure 11b shows the stress plot of the bolts showing the failure.

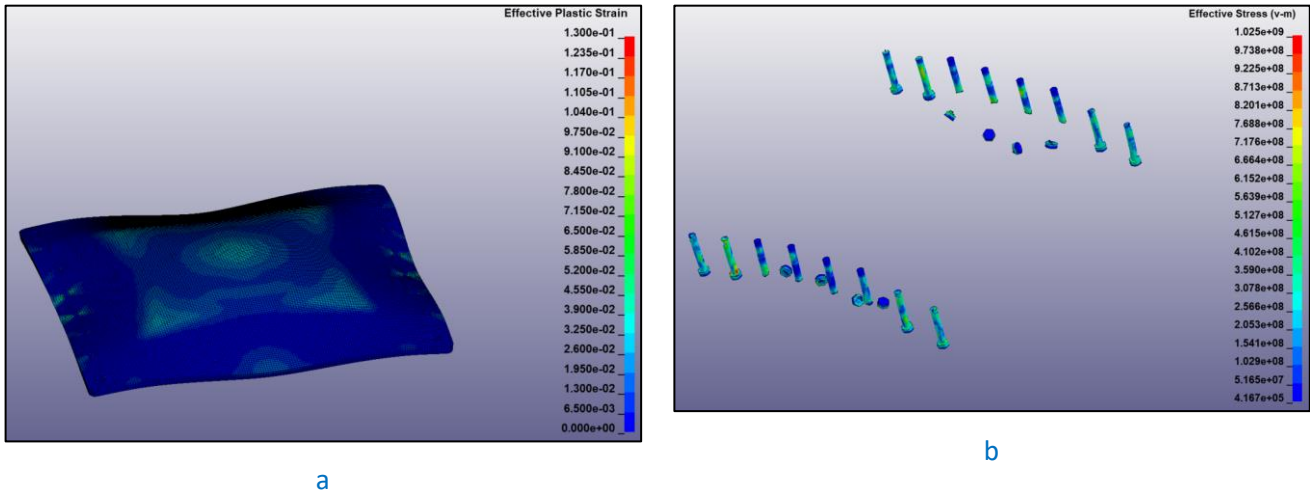


Figure 11: (a) Fringe plot of the Grade 2 simulation at peak deformation showing the stress distribution. (b) Stress plot of Grade 2 bolts showing 8 failures at the head of the bolt and 8 failures around the nut threads.

OPSEC# 6711

The plate deformation is then plotted. During the simulations, the bolts holding the target plate fractured for both the Grade 5 and Grade 2 bolts resulting in the plate detaching from the fixture. The deformation traces for both the Grade 5 and Grade 2 bolts were the same. This is due to the bolts failing from excessive loading early in the blast loading timeline. Figure 12 shows a plot of deformation versus time indicating the dynamic and permanent deformation. The permanent deformation is an average of the data points from 0.04s to 0.05s due to the reverberations in the plate and the later in time, the lesser reverberations occur. Recall the 0.05s was the end of the simulation. From this plot it is observed that the deformation from the Grade 8 simulation shows less peak dynamic deformation, but it rebounds very similar to the Grade 5 and Grade 2 simulations in addition to showing similar permanent deformation values.

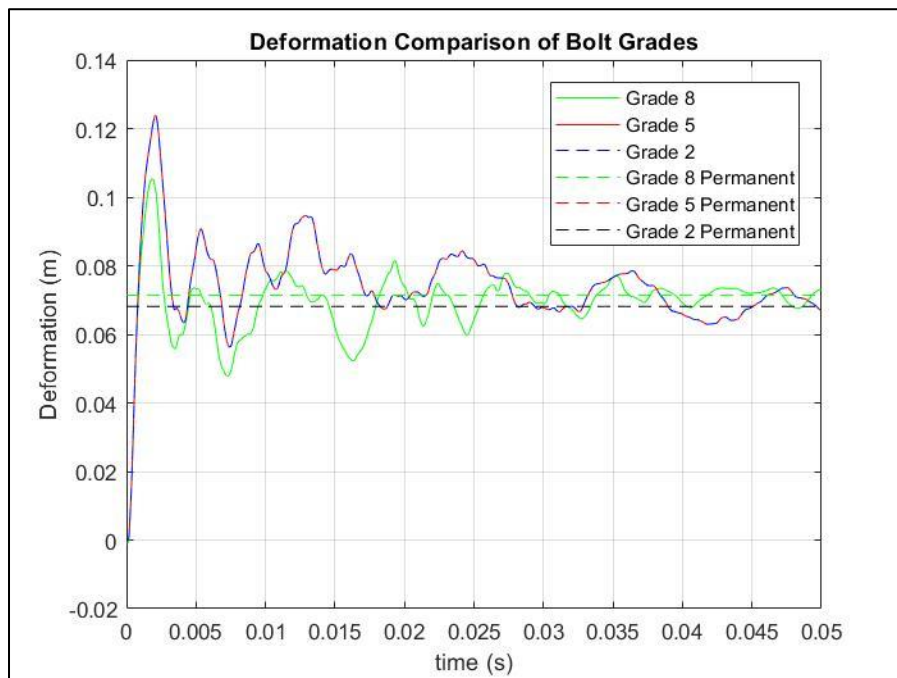
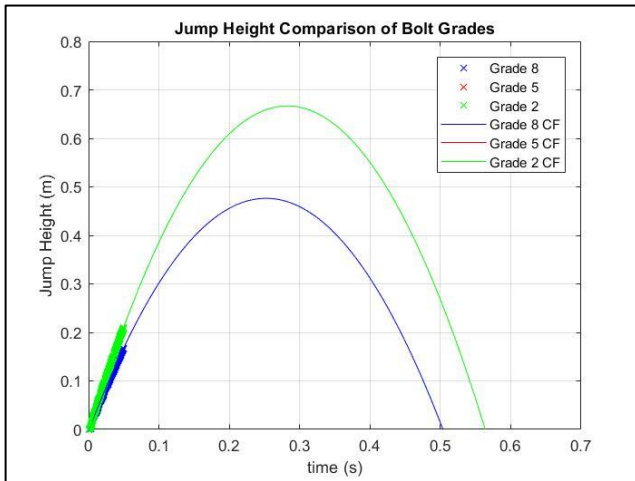
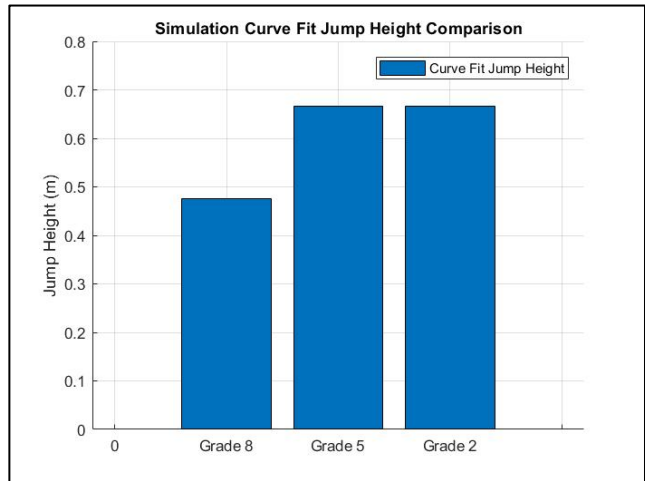


Figure 12: Dynamic and permanent deformation comparison between bolt grades. The Grade 8 dynamic deformation shows to be less than the Grade 5 and Grade 2, but the permanent deformation appears similar between all three grades.

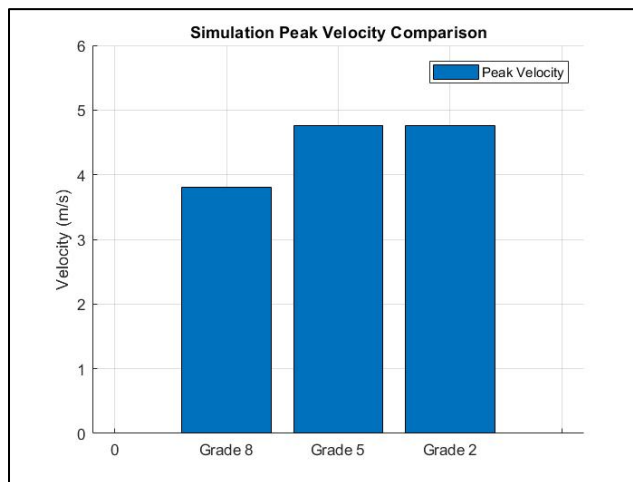
Next, the jump height comparison was made by collecting the nodal displacement and performing the curve fit analysis described in the "Parameters for Comparison" section. Figure 13a shows a plot of the jump height curve fit data where the Grade 5 and Grade 2 data lies on top of each other. Figure 13b shows a summary of the peak curve fit jump height values. Using equation 3, the velocity curves are generated. The peak velocity summary is shown in Figure 13c. Like the deformation plots, the Grade 5 and Grade 2 simulations showed the same jump height and velocities. The common theme between the two is the target plate falling off during the simulation at close to the same time. The target plate has separated from the fixture prior to the global motion, resulting in a very similar jump height for the Grade 5 and Grade 2 simulations. Therefore, the change in mass of the fixture without the target plate would result in the lighter flight assembly showing an increase in velocity and resultant peak displacement.



a



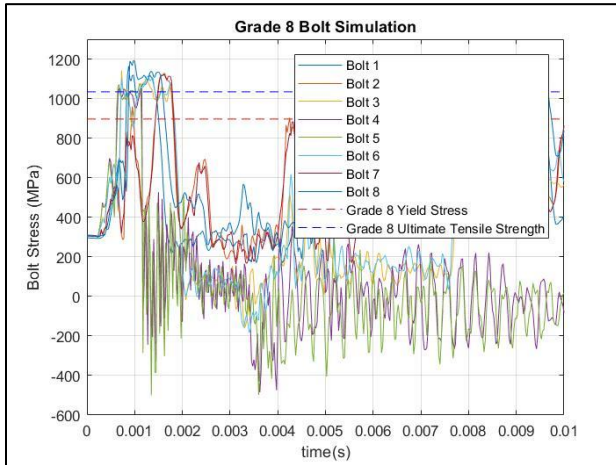
b



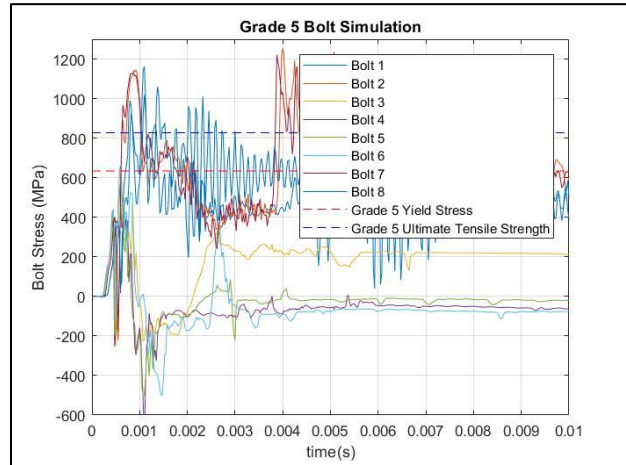
c

Figure 13: (a) Jump height curve fit data based on fixture displacement with the data points collected through t=0.050s for each and the curve fit tracking the full flight of t=0.5-0.6s. (b) Simulation peak jump height comparison. (c) Simulation peak velocity comparison. Both showing a reduction in jump height and velocity for the Grade 8 compared to the Grade 5 and 2.

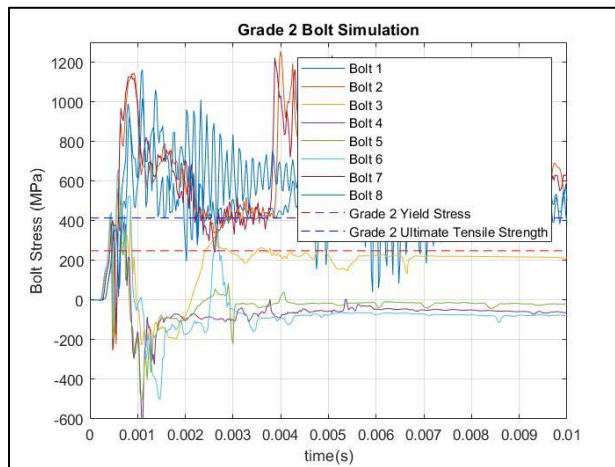
The bolt stresses are shown in Figure 14a-14c for the Grade 8, Grade 5, and Grade 2 bolts, respectively. The bolts are numbers 1 through 8 with bolts 1 and 8 on the outer edges and bolts 4 and 5 in the center. The data is collected from the elements identified in Figure 7d. Indicated on each plot is the Yield Stress and Ultimate Tensile Strength (UTS) for each grade. For the Grade 8 bolts, it is observed that some of the peak stresses exceed the UTS. This results in some of the bolts failing completely and some bolts having elemental failure in others. However, the target plate stayed on during the event. Figure 14a shows that some of the bolts failed but others did not. The Grade 5 and Grade 2 plots indicate a large overmatch in stress over the UTS. This caused failure of the bolts in different locations. However, even when the bolts failed and the target plate separated from the fixture, not all the stress was alleviated from the bolts in the simulation. This is an artifact in the simulation. A stress plot of this is shown in Figure 15a. In some cases, the bolts that did not fracture all the way through had element failures at the connection of the bolt to the nut resulting in the target plate separation. This is shown in Figure 15b. A closer look at the differences in the bolt load data show that the Grade 8 bolt peak loading occurs to maintain until approximately 2ms. The Grade 5 and Grade 2 simulations show the bolt loading to peak and drastically decrease at approximately 1ms. This indicates the bolt failure occurs prior to 1ms in the timeline. Knowing that the peak deformation has not occurred until the 1.9ms point in the timeline, the bolts offer little resistance to the deformation and at the point in time where peak dynamic deformation the bolts have failed.



a

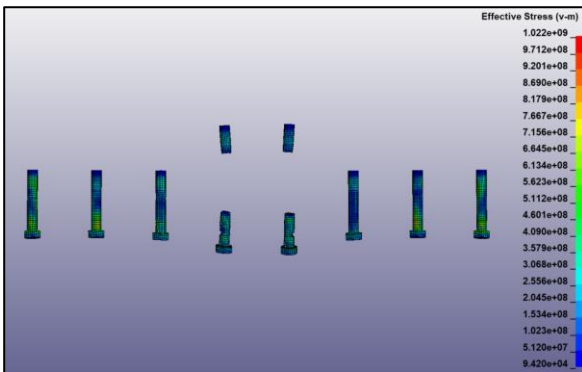


b

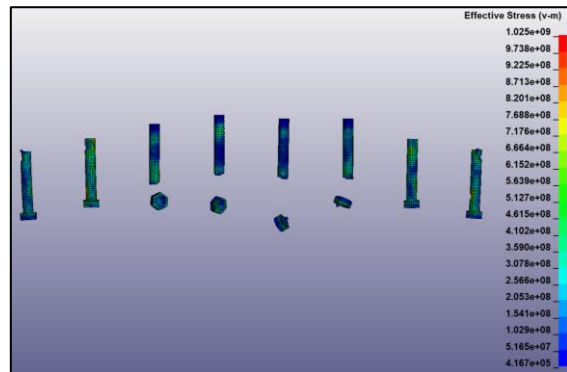


c

Figure 14: (a) Grade 8 bolt stresses showing loading just above UTS in some bolts with the loading occurring to 0.002s. (b) Grade 5 bolt stresses exceeding UTS and the loading ending at 0.001s. (c) Grade 2 bolt stresses showing loads well over UTS with the loading ending at 0.001s.



a



b

Figure 15: (a) Grade 8 bolts showing some failure in the center bolts with remaining stress in some bolts shown in yellow and orange on the shank of the bolt. (b) Grade 2 bolts showing multiple failures at the head and in the shank of the bolts.

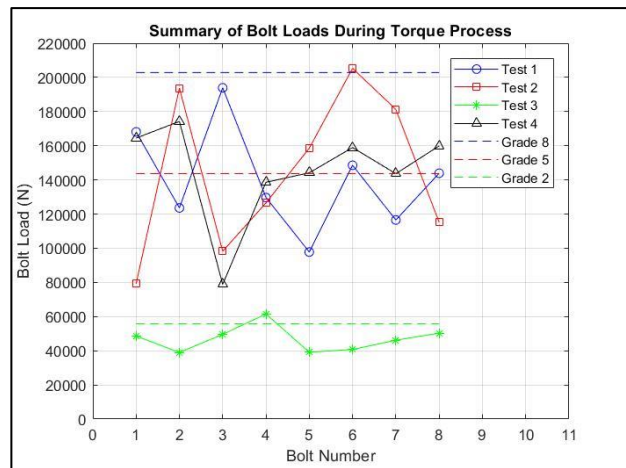
## Live Fire Testing

### Test Setup

For each test in the series, the target plate is installed and then torqued the specified amount based on the calculations. The instrumented bolts have their cores drilled out for the strain gauge instrumentation. As stated above, only 8 of the 16 bolts are instrumented. For the remaining bolts, a non-instrumented bolt was used. Figure 16a shows the instrumented and non-instrumented bolts next to each other. These dummy bolts are made following the same process as the instrumented bolts, except the strain gauge is omitted. This ensures the same size hole was drilled for each and therefore the cross-sectional area was identical between the two types of bolts. New bolts, washers, and nuts were used for each test. The bolt torques can fluctuate 30% in practice compared to analytical calculations. Accounting for both the reduced area and 30% fluctuation, Table 5 shows the estimated Proof Load and Torque values identified prior to the torquing procedure. During the torquing process, the loads were monitored and recorded using a live feed from the Dewetron system. Figure 16b shows the actual bolt loads based on location and a dashed line indicating the nominal proof load for each bolt grade. A fourth test was added to the test series and the torque value was increased to the maximum value of the Grade 8 bolt calculated in Table 5. Figure 16b indicates that this increase in torque had minimal effect on the observed load. The test was performed to see if any differences were observed with respect to the evaluation and comparison metrics.



a



b

Figure 16: (a) Instrumented bolts, shown with brass connector at the tip of the shank, compared to dummy bolts with just the hole drilled and no strain gauge mounted. (b) Bolt loads observed during torquing process with proof loads indicated for each grade. The Grade 8 bolts showed the largest variation and the Grade 2 showing the least variation compared to the target proof load.

**Table 5: Bolt Load and Torque Adjustments for Testing**

<b>Bolt Grade</b>	<b>8</b>	<b>5</b>	<b>2</b>
Nominal Proof Load (N)	210335.2	148987.4	57842.18
Nominal Torque (N*m)	895.4800	634.3000	246.2600
Instrumented Proof Load (N)	202822.5	143665.9	55776.19
Instrumented Torque (N*m)	863.5000	611.6400	237.4600
30% Minimum Proof Load (N)	141975.8	100566.2	39043.33
30% Maximum Proof Load (N)	263669.3	186765.7	72509.05
30% Minimum Torque (N*m)	604.4500	428.1480	166.2220
30% Maximum Torque (N*m)	1122.550	795.1320	308.6980

## Testing

A total of four tests were completed for this effort. The standoff for each test was nominally 457.2mm. A tolerance of plus/minus 6.35mm was required for each test. The standoff was measured at four locations around the steel containment cylinder to the surface of the target plate. To maintain a vertical jump height, the fixture is required to be leveled and the threat centered under the fixture. In the event the steel containment cylinder was not perfectly level, and the standoff tolerance was competing against the levelness of the fixture, *the levelness of the fixture took precedence over the standoff at that location.* Table 6 shows the test configuration, nominal standoff, standoff measurements recorded for each test and the average standoff for each test. Grade 8 HT is used to indicate the higher torque on the grade 8 bolts.

**Table 6: Standoff Measurements for each Test Number.**

<b>Test Number</b>	<b>Test Configuration</b>	<b>Nominal Standoff (mm)</b>	<b>Location 1 (mm)</b>	<b>Location 2 (mm)</b>	<b>Location 3 (mm)</b>	<b>Location 4 (mm)</b>	<b>Average (mm)</b>
1	Grade 8	457.2	458.8	463.6	447.7	452.4	455.6
2	Grade 5	457.2	455.6	463.6	449.3	458.8	456.8
3	Grade 2	457.2	458.8	460.4	452.4	449.3	455.2
4	Grade 8 HT	457.2	460.4	463.6	452.4	452.4	457.2

## Results

Test 1 did not show any cracking or failure of the target plate. All 16 of the bolts remained intact and the target plate remained attached after the test. Figures 17a and 17b show the back and the front surfaces of the deformed target after the event. The instrumented bolt strain gauge connectors broke off the bolts during the test, but the wires remained connected. Even though the bolts didn't break, they did yield and deform during the test. Figure 17c shows the condition of the instrumented bolts after the test. Figure 17d shows the bolt loads recorded from the test. After the yielding of the bolt, the strain gauge has limited accuracy. Therefore, if the data clipped due to yielding only the data recorded until the first indication of data clipping was utilized.



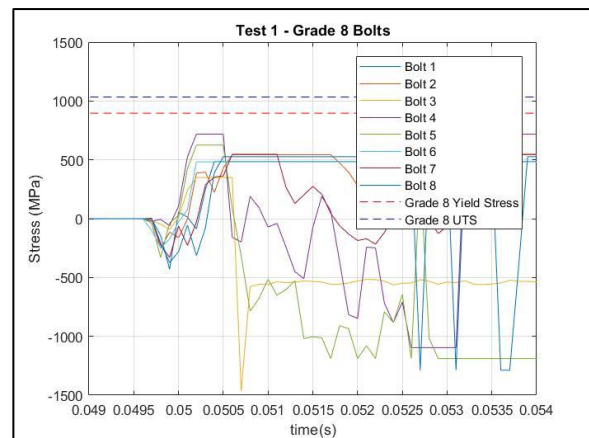
a



b



c



d

Figure 17: (a) Test 1 back face of deformed target with no failure observed. (b) Test 1 strike face of deformed target showing deformation and warping of the target plate. (c) Instrumented grade 8 bolts deformed after test showing yielding but no failures. (d) Bolt loads recorded during Test 1 showing an initial ramp up and then clipping due to the yielding of the bolts.



OPSEC# 6711

Test 3 did not show any cracking or failure in the target plate. All 16 bolts failed causing the target plate to fall off during the test. Figure 19a shows the fixture and target after the test. Figure 19b shows the deformed surface of the target plate. During the failure of the instrumented bolts, the DAS malfunctioned and failed to collect the data. Figure 19c shows the condition of the instrumented bolts after the test. Figure 19d shows a zoomed in picture showing the necking and cupped failures indicative of a tensile failure in the bolts.



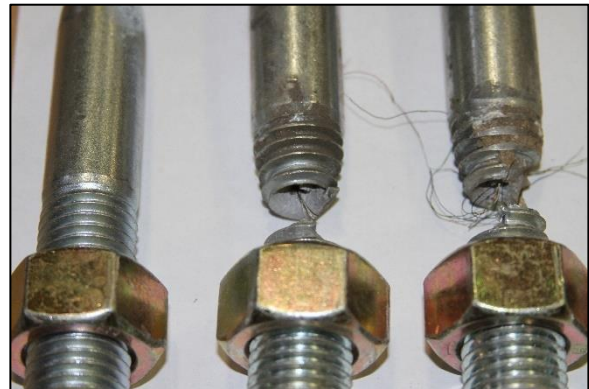
a



b



c



d

Figure 19: (a) Fixture after Test 3 showing target plate on ground after landing. The target centered under the fixture after the event indicates a strictly vertical flight of the fixture. (b) Deformed target plate after falling off fixture with no failures observed. (c) Failed instrumented grade 2 bolts after test with all bolts failing due to tensile failures. (d) Close in view of Grade 2 bolts showing ductile tensile failures indicated by necking and cup failure surfaces.

Test 4 did not show any cracking or failure of the target plate. 12 of the 16 bolts remained intact and the target plate remained attached after the test. Figures 20a and 20b show the back and front surfaces of the target plate after the test. Figure 20c shows the condition of the instrumented bolts after the test. In this case, the four bolts that failed (Bolt 1, Bolt 4, Bolt 5, and Bolt 8) were non-instrumented bolts. Figure 20d shows the failed non-instrumented bolts. Figure 21 shows a summary of the bolt loads.



a



b



c



d

Figure 20: (a) Test 4 back face of deformed target showing no failures of the plate. (b) Test 4 strike face of deformed target showing warping and multiple bolt failures. (c) Instrumented Grade 8 bolts deformed after test. (d) Dummy bolts that fractured during the test showing failures at the center and outer edges.

OPSEC# 6711

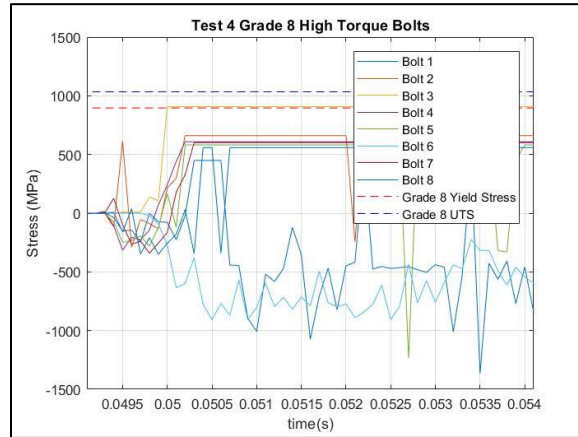


Figure 21: Bolt loads recorded during Test 4 showing clipping at the yielding of the bolts event when the stresses were below the yield stresses of the bolts.

After each test, the permanent deformation was measured. Figure 22 and Table 7 show a summary of the deformation from the four tests. From the table, the data shows a maximum of 8% variation from the mean.

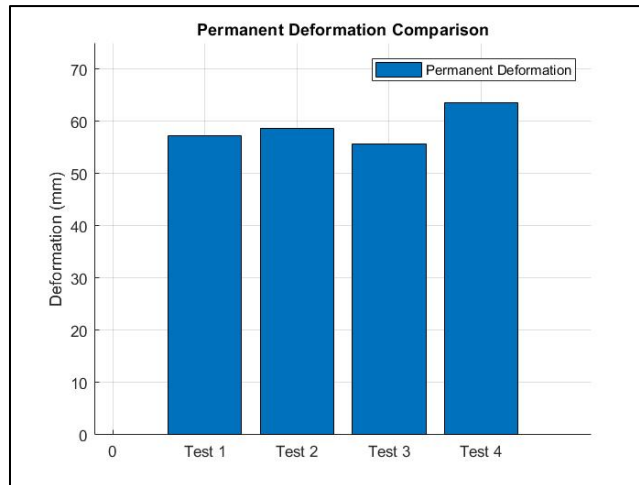
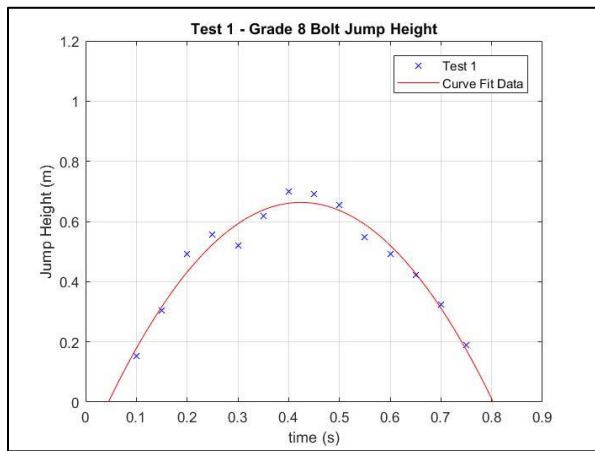


Figure 22: Comparison of permanent deformation recorded during test series indicating small differences between each test.

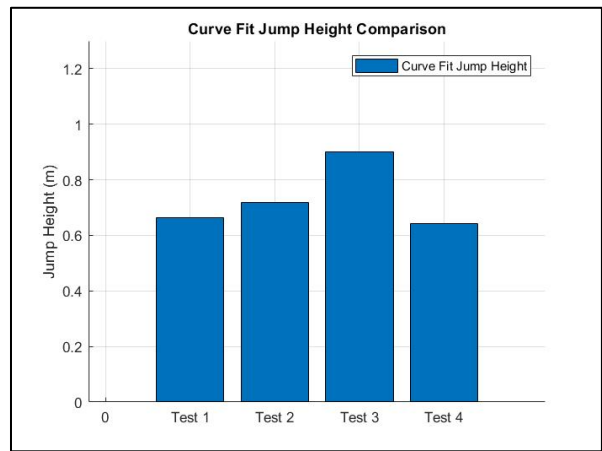
Table 7: Summary of Permanent Deformation Values from Testing

Test Number	Permanent Deformation (mm)
1	57.15
2	58.74
3	55.56
4	63.50

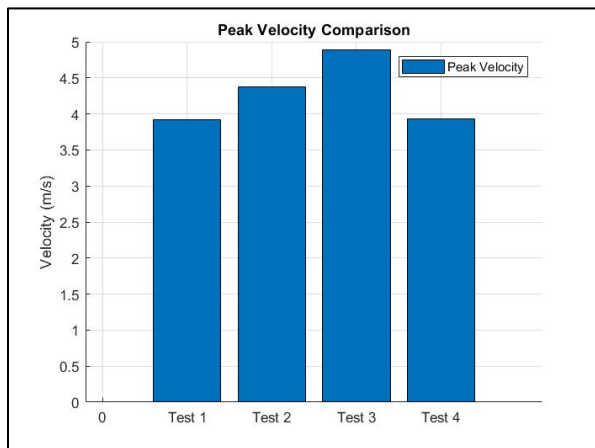
Next the high-speed video was analyzed, and the jump height data was processed. Figure 23a shows an example of the data points collected from the high-speed video and the curve fit analysis performed. The curve fit data for each test is contained in Appendix B. Figure 23b shows a summary of the peak jump height observed based on the curve fit data analysis for each test. Next the peak velocity was determined using Equation 3 and is shown in Figure 23c. The peak velocity was used in Equation 4 to determine the impulse for each test, which is shown in Figure 23d. As stated above, if the target plate fell off as it did in Test 3, then the target plate mass was omitted from the total weight.



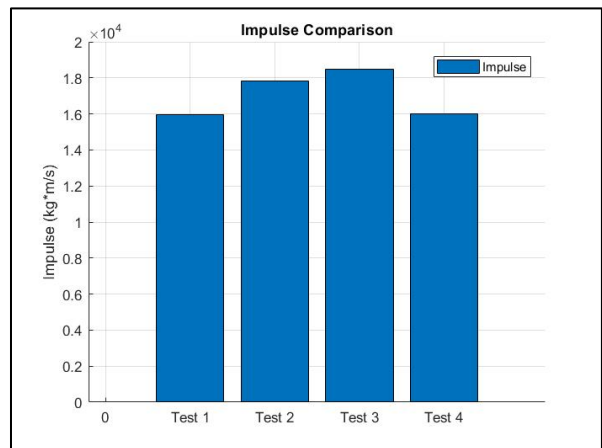
a



b



c



d

Figure 23: (a) Example of jump height curve fit analysis showing the data points collected throughout the event and the curve fit based on the test data. (b) Curve fit jump height comparisons from testing. (c) Peak velocity comparison of test series. Showing the highest jump height and largest velocity in Test 3 when the target plate fell off. (d) Impulse comparison from test series accounting for the target falling off during Test 3.

## Results Summary, Comparisons of Testing to Simulation, and Analysis

The data from the live fire testing and simulations were then compared to each other to understand similarities and differences between the two. Figure 24a shows a permanent deformation plot for both the testing and simulations. Test 1 and Test 4 are compared back to the same simulation data for the Grade 8 bolts as the only difference was the torque value. Figure 24b shows a comparison of the velocities for both the tests and the simulations. The permanent deformation values were higher for the simulation versus the testing. This could be a result of a multitude of different factors including the duration selected for the simulation, the amount of data points used to take the average to remove the plate reverberations, the material model used, and the mechanical properties of the target plate. Since the simulation deformation is an average and is recorded at the 50ms point in the timeline it is expected for there to be slight differences compared to the testing where a single value is acquired after the complete test has occurred. The error for the testing and the simulation was 8% and 3% respectively. When compared together the simulations showed a difference of 12-24% where the simulation was consistently higher than the testing. This error is mostly likely a contribution of the factors above as well as slight differences in material models from the Johnson-Cook constitutive parameters and the as-tested mechanical properties of the target plates. Previous efforts have shown similar differences in material responses as the deformation and failure predictions is a very complex phenomena to replicate on a case-by-case basis.

The target plate separating from the fixture prior to the global response has already shown to alter the velocity observed. This was consistent between both the simulation and testing. Therefore, an error from test to test or simulation to simulation was not performed as it would show a large variance. Comparing the simulation to the testing the difference was significantly closer showing only 3-9%. There is no consistent pattern to simulations being higher than testing or vice versa.

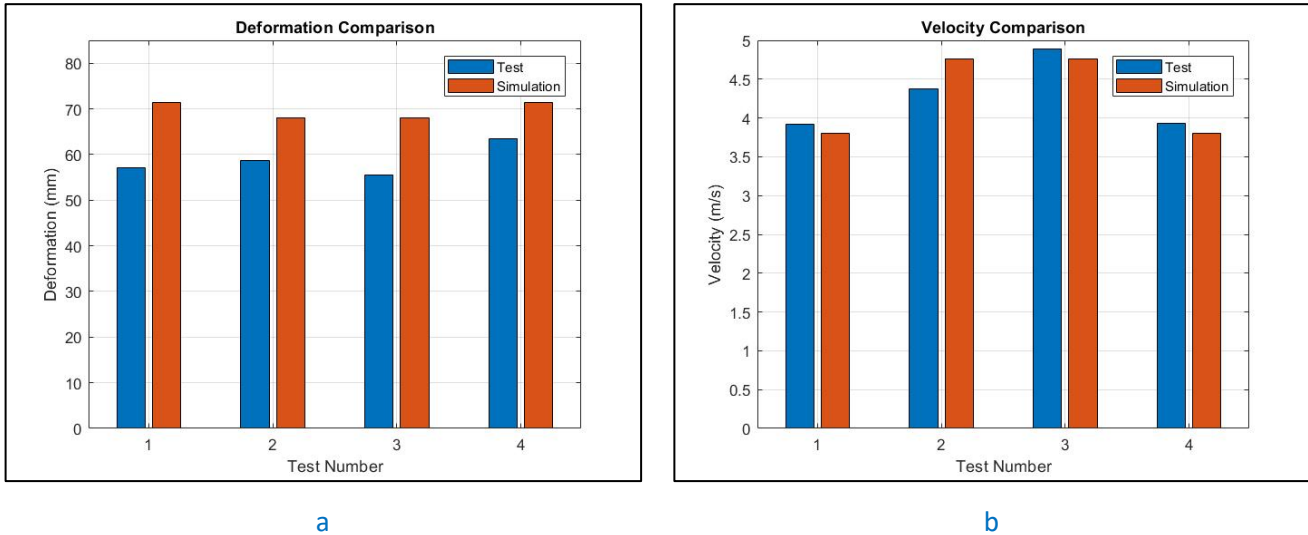


Figure 24: (a) Deformation comparison between test and simulations. (b) Velocity comparison between test and simulations.

Next the impulse values were compared. Conventionally the impulse is used to verify the load imparted on the structure. However, it only accounts for the total mass of the collective flight assembly and the peak velocity observed. Figure 22c shows the comparison for both the tests and simulations. However, both the simulations and tests showed differences in deformation that changes how the load is used. The error for each calculated from the mean is 8.3% in testing and 7.5% for the simulation. The impulse for the testing and simulations individually having less than a 10% error indicates a consistent setup for each respectively. Similar testing has shown to have a 11-13% in buried soil and the steel containment cylinder is expected to have a more consistent imparted load profile. This data follows that trend. Comparing the simulations to the testing that difference was 1-3% which shows great correlation between the two.

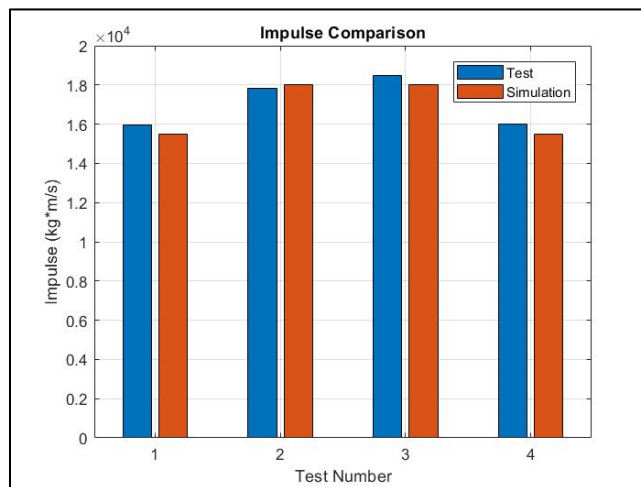


Figure 25: Impulse comparison between test and simulations.

OPSEC# 6711

Leveraging the energy equations shown in Equations 5-8, a more detailed comparison can be made. Figure 26 shows the comparison of the total energy between the testing and the simulation. The error for each calculated from the mean is 5.2% for testing and 1.6% for the simulation. Table 8 shows a breakdown of the energy contributions from each major factor. As stated above, the main differences between the energy conservation method and the impulse method are the inclusion of the differences in bolt strengths and differences in target plate deformation. From Table 8, the contributions of the plate deformation clearly dominate that of the bolts. Through the inclusion of the plate deformation the error was reduced to almost in half for each independently. However, the deformation also brings in the 12-25% error between the simulation and testing. Therefore, the difference between the simulation and testing was 9-19%. The increased energy in the simulations versus the testing is attributed to the target plate material model as this directly effected the deformation values. The trend of the simulation values being higher than the testing is consistent for both the permanent deformation and the total energy while the velocity and impulse showed no discernable trend.

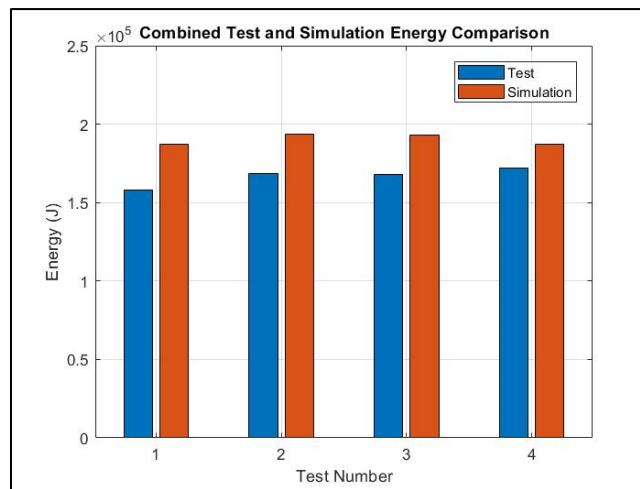


Figure 26: Combined test and simulation energy comparison.

OPSEC# 6711

Table 8: Energy Breakdown for Test and Simulation

Test	Bolt Energy (J)	Deformation Energy (kJ)	Kinetic Energy (kJ)	Total Energy (kJ)
1	423.86	126.10	31.242	157.76
2	214.37	129.60	38.977	168.79
3	32.450	122.60	45.212	167.84
4	423.86	140.11	31.477	172.01
Simulation				
1	423.86	157.54	29.448	187.41
2	214.37	150.26	42.922	193.40
3	32.450	150.26	42.922	193.21
4	423.86	157.54	29.448	187.41

## Conclusions

The simulations provided an opportunity to examine the blast loading timeline to understand the sequence in which the major components were affected by the explosive loading. The bolt loading was very close to the initial peak pressure from the blast. This indicates that any bolt fracture occurs during the initial ramp up of the deformation. However, for the grade 8 bolt simulation the timeline did show that the bolt loading overlapped the deformation curve almost until the peak deformation was observed. This timeline also showed that the peak deformation happens before any liftoff of the fixture indicating that the deformation and the global movement of the fixture are decoupled. The liftoff timeline showed that the bolts break, and the target plate decouples from the fixture before or right at the beginning of the lift off and therefore it can be removed from the total mass displacing during the global motion during the impulse and energy conservation analysis.

The simulations predicted a reduction in dynamic deformation when the bolts held the target plate to the fixture versus when the plate falls off. However, the permanent deformation was very similar. This was not able to be realized during the test series but should be investigated further, especially if dynamic deformation is the driver for an occupant injury at a particular location in a vehicle.

Although a direct velocity can be extracted from the simulations, processing the simulation data the same way as the test data showed to be an accurate comparison tool, thus reducing the error between testing and simulations when compared to methods such as rigid body velocity measurements.

In all the simulations, the bolt loads peaked higher than the UTS. However, the Grade 5 and Grade 2 showed larger overmatch to the loads resulting in element failure of the bolts. This indicates some level of element failure, but this is akin to the stretching or necking observed in testing. This may not directly indicate a complete bolt failure.

Bolt ratings are specified as a minimum in practice. It is assumed that the bolts used in testing would be stronger than the minimum. This likely plays a role in when and how the bolt failures occurred in testing versus the simulations.

The bolt torque values showed a large variance, consistent with literature. The bolt torque did not have a significant contribution to the testing. Test 4 showed a higher permanent deformation than Test 1, however the measured load at the bolts during the torquing process did not show any measurable difference in axial load.

The instrumented bolts provided valuable information during this test series. The initial loading up until the bolts either fractured or yielded gave validity to the loading process of the simulation.

The variation observed during the torquing process was significant. Between the 8 bolts the error ranged from 17% to 45%, with the error being reduced at the lower torque values. Obtaining the target load for the grade 8 bolts was very difficult. Even with the increase in bolt torque it showed little difference in the load. This increase in bolt torque did show to have a negative effect on deformation and showed an increase in the number of bolt failures observed compared to test 1, the original grade 8 bolt test. Therefore, it is recommended that the torque values set during the design phase of an underbody kit should be chosen such that it is on the lower end of the torque window to ensure that the variation does not weaken the bolt during the underbody kit installation process.

The permanent deformation measurements were consistent between each test in the series and each simulation. The simulations showed consistently higher values than the testing. The material models used for this effort have proven to be the most accurate depictions of blast and ballistic events. However, they are still based on experimental testing of purchased production material. Therefore, manufacturing variances during the material manufacturing process greatly contribute to the accuracy of the model used. Modeling and simulation are often used as a predictor prior to testing and having a conservative model may be beneficial prior to testing.

The explosive loading process is often equated using impulse. In both testing and simulations, this resulted in a 7.5-8.3% error. This is used to understand the test to test or simulation to simulation variance. The use of energy conservation methods, including those developed by P.S. Westine *et al* provided a method for comparing similar tests or simulations because it accounts for changes in deformation and velocity. The error observed using this method was 1.6%-5.3%.

Based on the energy conservation method, the energy absorbed through the strain energy of bolts are orders of magnitude less than the strain energy of the target plate and the kinetic energy of the fixture. Therefore, the actual energy absorbed by the bolts contributes very little to the energy usage process. In most cases the equation can be simplified to include only the target plate deformation and the kinetic energy resulting from the global motion of the fixture or vehicle.

The use of different grade bolts did not play a significant role in the permanent deformation. However, retaining the target plate, or underbody kit on the vehicle, during the test reduces the global velocity observed, even when the target plate is 7% of the overall system weight. The simulation and testing both showed a reduction in global velocity of 0.96-0.97m/s, 22% of the average global velocity.

In underbody kit design, ratios of potential underbody kit weights to vehicle weight should be developed early on to determine if the kit staying on the vehicle would be beneficial. Then, a bolted joint configuration should be determined based on both the low amplitude-high cycle and the high amplitude-low cycle loading should be devised. Once that is determined, an appropriate torque sequence and value should be determined keeping the targeted axial load values on the lower end of the design window to ensure the full strength of the bolt is utilized during the blast loading process.

## **Future Work**

Additional testing with the ability to record dynamic deformation is required to determine if the decrease in dynamic deformation in the simulation phase would be observed in testing as well. This would provide a better understanding to the differences in peak dynamic deformation observed in the simulation portion of this effort. If the dynamic deformation were to show a reduction, as was observed in the simulation, the use of higher-grade bolts to keep the target plate attached during the test would have an additional benefit aside from the reduction in global velocity.

The use of energy conservation versus impulse could be leveraged for other test series as a more accurate method for comparing similar test events. This is particularly useful during armor development when repeat tests are performed and an understanding of test-to-test variance is tied to design space.

The blast loading timeline should be compared to buried blast tests to understand any differences and the impact of those differences. It is presumed that the addition of the coupling between the explosive and soil will slow down the initial peak pressure on the target. What is unknown is whether the rest of the timeline shifts to the right or if there is overlap not previously observed.

## Works Cited

1. Cheeseman, B., Lynch, M., (2018) Learning the Lessons of History: U.S. Army Efforts on Underbody Blast Mitigation and Elimination of this Threat for Future Forces. US Army Research Laboratory.
2. Burgess, V., Kankanalapalli, S., (2021) Effects of Explosive Charge Dimensions on Vehicle Hull Structures. GVSC-TR-30042. DTIC AD1143947.
3. Shigley, J., Mischke, C., (2002) Mechanical Engineering Design (5<sup>th</sup> ed.) McGraw Hill.
4. Bickford, J., Nassar, S., (1998) Handbook of Bolts and Bolted Joints (1<sup>st</sup> ed.) Marcel Dekker, Inc.
5. Carmichael, C., (1950) Mechanical Engineer's Handbook, Design and Production (12<sup>th</sup> ed.) Wiley.
6. Strainsert (2006) Strainsert 2006 catalog, Force sensing bolts and studs.
7. Socks, A., (2022) Combat Vehicle Prototype (CVP) Foundational Armor Bolt Optimization Technical Report. GVSC-TR-29986.
8. Mathworks (2017b) MATLAB software.
9. Westine, P., *et al* (1975) Energy Solutions for Predicting Deformations in Blast-Loaded Structures. DTIC ADA022333.
10. LSTC (2018) LS-DYNA software. <https://www.lstc.com/products/ls-dyna>.
11. Altair (2017) Hyperworks software. <https://www.altair.com/hyperworks/>.
12. Lee, E., Horning, H., Kury, J., (1968) Adiabatic Expansion of High Explosives Detonation Products, Lawrence Livermore National Laboratory, University of California, Livermore. TID 4500-UCRL50422.
13. Livermore Software Technology Corporation (LSTC) (2012) LS-DYNA Keyword User's Manual, Volume II Material Models.
14. Johnson, G., Cook, W., (1983) A Constitutive Model and Data for Metals Subjected to Large Strains, High Strain Rates, and High Temperatures.
15. Johnson, G., Holmquist, T., (1992) A computational Constitutive Model for Brittle Materials Subjected to Large Strains.
16. Babu, V., Kulkarni, K., Kankanalapalli, S., Khatib-Shahidi, B., (2018) Comparative Analysis of Occupant Responses between LS-DYNA Arbitrary Lagrange in Euler and (ALE) and Structured-ALE (S-ALE) Methods. DTIC AD1055066.
17. LSTC (2018) LS-PrePost V4.3.20.

## **Appendix A: Strainsert Strain Gauge Calibration Example**

### STRAINERT CALIBRATION CERTIFICATE

12 Union Hill Rd. West Conshohocken, PA 19428

Transducer: Special Load Sensing Bolt, #92620A966	Q-26210-A
	Strainert Job No.
	Date: 04/16/2020
	Sign: E. Pettiford

Model (SPL-FB) 1-8NC x 6"-lg.(Grade 8) (350 Ohms/150 Deg °F) C To K(LO) So	Type: C (Microtech DR-4S-4H) Ins. Res.: Over 10,000 megohms
Service Temp.: 150 Deg. F Max.	

CAL TEMP: 72 Deg F	Cal Date: 04/16/2020	S/N: Q26210A-9
R.H. %: 24	Cal Due: 04/16/2021	
MODE: TENSION		CABLE LENGTH: 75.0 FT

TEST LOAD LBS	STRAIGHT	DEVIATIONS-uv/V			REP
	LINE				
	SIGNAL	RUN-1	RUN-2	RUN-3	uv/V
	mv/V				
0	0.000	0.0	0.0	0.0	0.0
12,400	0.917	-6.5	-7.0	-7.0	0.5
24,800	1.834	-8.5	-8.5	-8.5	0.0
37,200	2.751	-7.0	-6.5	-7.0	0.5
49,600	3.668	-1.0	-0.5	-1.0	0.5
62,000	4.585	8.5	9.0	9.0	0.5
0	0.000	0.0	0.0	0.0	0.0

CALIBRATION ANALYSIS:

NON-LINEARITY:	9.0 PARTS IN	4,585 = 0.20%
REPETITION:		
LOADING:	0.5 PARTS IN	4,585 = 0.01%
ZERO LOAD:	0.0 PARTS IN	4,585 = 0.00%
MAX LOAD:	0.5 PARTS IN	4,585 = 0.01%
END POINT:	9.0 PARTS IN	4,585 = 0.20%

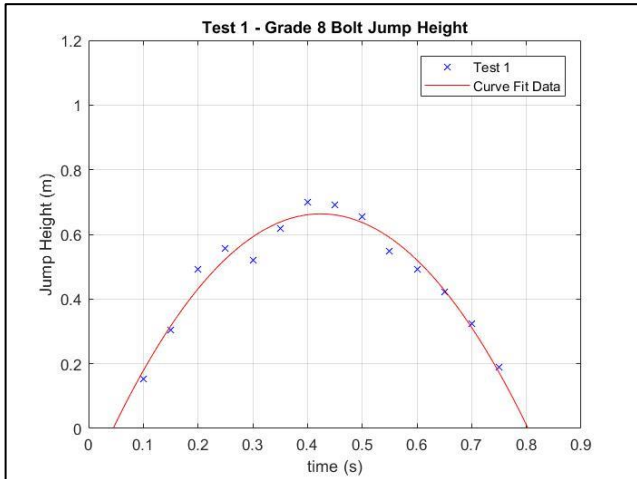
  

SHUNT CAL: 27,200 Ohms connected E+ to S+ = +47,017 lbs  
 Calibration traceable to NIST

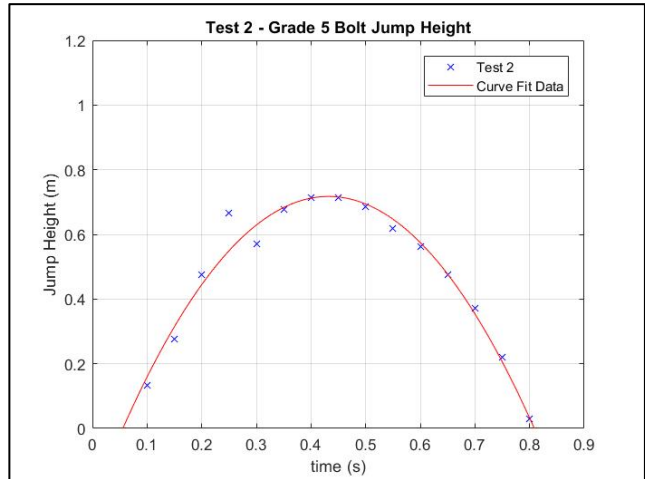
Page 1 of 1

Figure 27: Strainert strain gauge bolt calibration example. Calibration performed using SAE unit system and loads converted to SI during analysis stage.

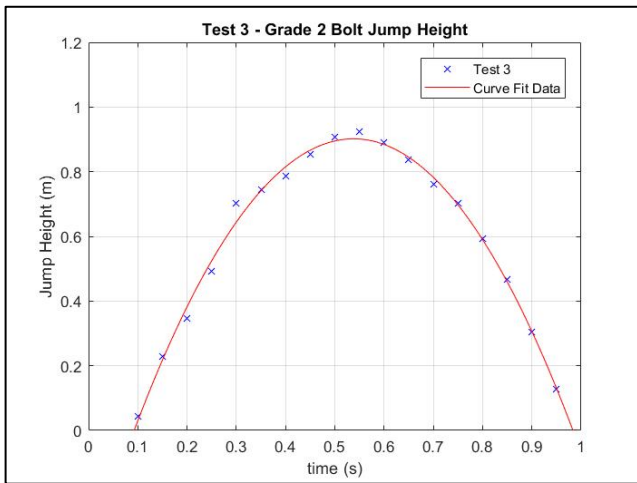
## **Appendix B: Jump Height Curve Fit Analysis**



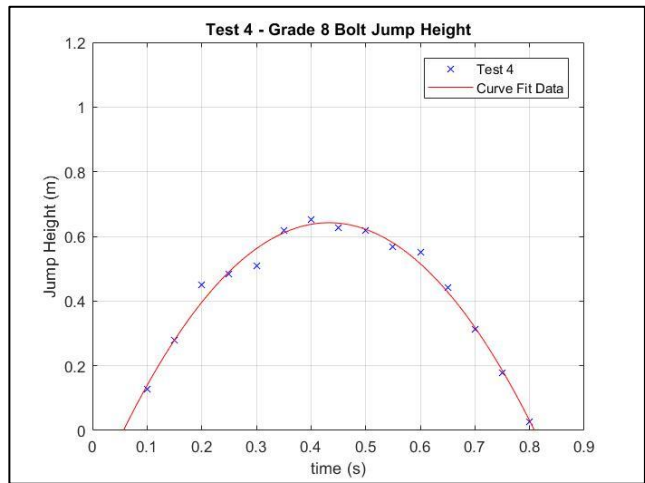
a



b



c



d

Figure 28: (a-d) Jump height analysis for each test. Showing (a) the Grade 8, (b) the Grade 5, (c) the Grade 2, and (d) the Grade 8 High Torque.